Available online at www.sciencedirect.com
ScienceDirect
Tectonophysics 426 (2006) 295–317
TECTONOPHYSICS
www.elsevier.com/locate/tecto

Kinematics of the Iberia–Maghreb plate contact from seismic moment tensors and GPS observations

Daniel Stich [a,*], Enrico Serpelloni [b], Flor de Lis Mancilla [c], Jose Morales [c]

[a] *Istituto Nazionale di Geofisica e Vulcanologia, Sezione di Bologna, Italy*
[b] *Istituto Nazionale di Geofisica e Vulcanologia, Centro Nazionale Terremoti, Bologna, Italy*
[c] *Instituto Andaluz de Geofisica, Universidad de Granada, Spain*

Received 19 January 2006; received in revised form 9 August 2006; accepted 10 August 2006
Available online 28 September 2006

Abstract

The Iberian Peninsula and the Maghreb experience moderate earthquake activity and oblique, ~ NW–SE convergence between Africa and Eurasia at a rate of ~ 5 mm/yr. Coeval extension in the Alboran Basin and a N35°E trending band of active, left-lateral shear deformation in the Alboran–Betic region are not straightforward to understand in the context of regional shortening, and evidence complexity of deformation at the plate contact. We estimate 86 seismic moment tensors (M_W 3.3 to 6.9) from time domain inversion of near-regional waveforms in an intermediate period band. Those and previous moment tensors are used to describe regional faulting style and calculate average stress tensors. The solutions associated to the Trans-Alboran shear zone show predominantly strike-slip faulting, and indicate a clockwise rotation of the largest principal stress orientation compared to the regional convergence direction (σ_1 at N350°E). At the N-Algerian and SW-Iberian margins, reverse faulting solutions dominate, corresponding to N350°E and N310°E compression, respectively. Over most of the Betic range and intraplate Iberia, we observe predominately normal faulting, and WSW–ENE extension (σ_3 at N240°E). From GPS observations we estimate that more than 3 mm/yr of African (Nubian)–Eurasian plate convergence are currently accommodated at the N-Algerian margin, ~ 2 mm/yr in the Moroccan Atlas, and ~ 2 mm/yr at the SW-Iberian margin. 2 mm/yr is a reasonable estimate for convergence within the Alboran region, while Alboran extension can be quantified as ~ 2.5 mm/yr along the stretching direction (N240°E). Superposition of both motions explains the observed left-lateral transtensional regime in the Trans-Alboran shear zone. Two potential driving mechanisms of differential motion of the Alboran–Betic–Gibraltar domain may coexist in the region: a secondary stress source other than plate convergence, related to regional-scale dynamic processes in the upper mantle of the Alboran region, as well as drag from the continental-scale motion of the Nubian plate along the southern limit of the region. In the Atlantic Ocean, the ~ 3.5 mm/yr, westward motion of the Gibraltar Arc relative to intraplate Iberia can be accommodated at the transpressive SW-Iberian margin, while available GPS observations do not support an active subduction process in this area.

Keywords: Moment tensor inversion; Stress tensor inversion; GPS observations; Plate boundary; Continental shear zone; Iberia–Maghreb region

1. Introduction

The Iberia–Maghreb region, comprising Spain, Portugal and the northern parts of Morocco and Algeria, is situated at the obliquely convergent African–Eurasian plate contact. Present-day convergence between Africa

* Corresponding author.
E-mail address: daniel@bo.ingv.it (D. Stich).

0040-1951/$ - see front matter © 2006 Elsevier B.V. All rights reserved.
doi:10.1016/j.tecto.2006.08.004

(i.e. Nubian plate) and Iberia occurs at rates of ~ 5–6 mm/yr, and with approximately NW–SE to WNW–ESE shortening direction (DeMets et al., 1994; Calais et al., 2003; McClusky et al., 2003; Serpelloni et al., submitted for publication). Plate convergence coexists with extensional processes in the westernmost Mediterranean sector (e.g. Platt and Vissers, 1989; Docherty and Banda, 1995; Comas et al., 1999; Jolivet and Faccenna, 2000), with both processes interacting to produce complex tectonic deformation over the Iberia–Maghreb region. Earthquakes (Fig. 1) are concentrated along regional-scale WSW–ENE lineaments in northern Algeria and easternmost Atlantic Ocean, presumably marking two segments of the convergent Africa–Eurasia plate boundary. In between, at the contact of Morocco and Spain, seismicity is distributed over a more than 400 km wide zone, and characterized by lower magnitudes (usually smaller than 5.5), compared to the adjacent sections (Buforn et al., 1995). These characteristics suggest a diffuse partitioning of plate convergence strain, and complicate the definition of a plate boundary between Morocco and Spain.

Seismotectonics of the Iberia–Maghreb region has been treated in numerous focal mechanism studies. As the number of regional seismic broad-band stations is increasing, the methodological focus turns from evaluating first motion polarities (recent studies and compilations e.g. Mezcua and Rueda, 1997; Bezzeghoud and Buforn, 1999; Borges et al., 2001; Buforn et al., 2004) towards regional waveform inversion, including moment tensor studies of selected events (Thio et al., 1999; Dufumier et al., 2000; Mancilla et al., 2002; Buforn and Coca, 2002), as well as systematic assembling of regional moment tensor catalogues (Pondrelli et al., 2002; Braunmiller et al., 2002; Stich et al., 2003; Rueda and Mézcua, 2005). These studies report a number of different regional faulting trends along the plate boundary zone: Northern Algeria is characterized by predominantly reverse faulting under ~ NNW–SSE compression. At the SW-Iberian margin, reverse and strike-slip faulting occur under ~ NW–SE compression. In the Alboran Basin and southern Spain, strike-slip and normal faulting prevail, suggesting interplay of extensional tectonics and

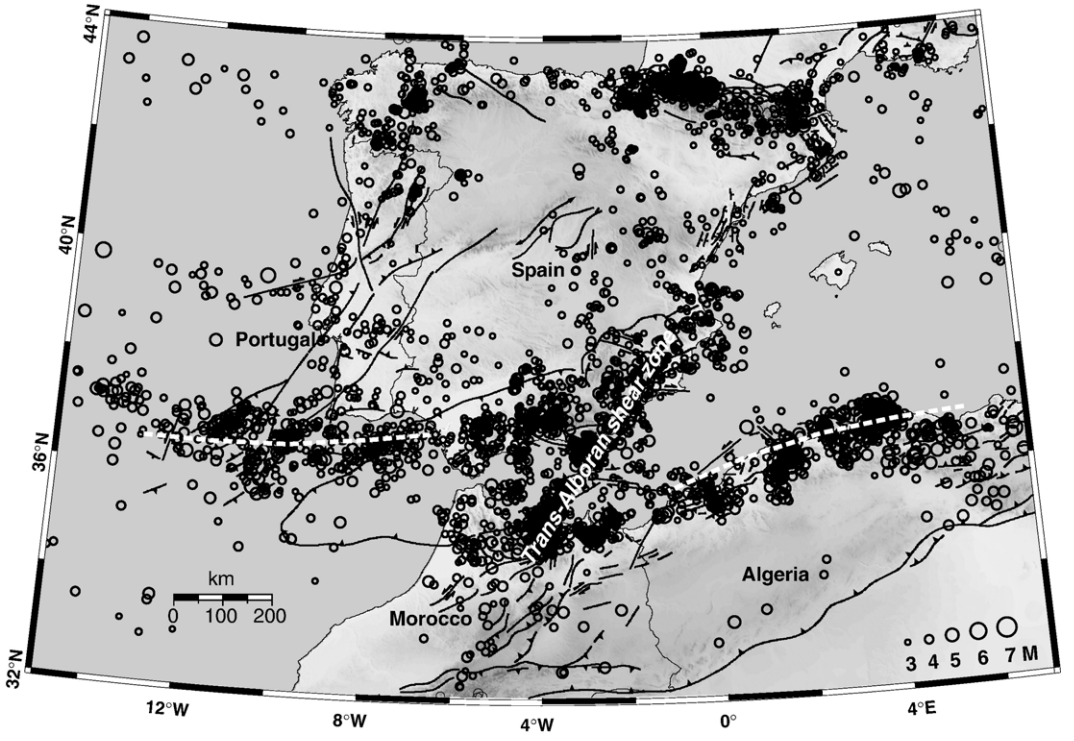

Fig. 1. Seismicity of the Ibero–Maghrebian region projected on the map of active and potentially active faults. Epicenters of earthquake with local magnitude ≥3 (scale on lower right) are taken from the NEIC catalogue (http://neic.usgs.gov). Neotectonic faults (grey) are redrawn from the Geodynamic map of the Mediterranean compiled in the frame of the Commission for the Geological Map of the World (http://ccgm.free.fr). Seismicity is relatively focused at the Algerian and SW-Iberian margins (highlighted by dashed white lines), but more diffuse between Morocco and Spain, where the left-lateral TASZ is the main regional-scale active structure. Relevant seismicity is also observed in the Pyrenees and in several intraplate areas on and around the Iberian Peninsula. In the Atlantic Ocean and inland Africa the seismicity appears to be depleted of small, magnitude 3 earthquakes, reflecting limits of catalogue completeness.

Nubia–Eurasia plate convergence along this section of the plate contact (Mezcua and Rueda, 1997; Bezzeghoud and Buforn, 1999; Stich et al., 2003).

The extension of the Alboran region during ongoing African-European convergence has been related to very diverse geodynamic processes, including a continental scale thermal mantle source that drives rifting from the Rhine–Bresse–Rhône Graben system into the westernmost Mediterranean (Hoernle et al., 1995), and to regional scale recycling of lithosphere into the mantle, with the proposed mechanisms being active continental subduction (Morales et al., 1999), delamination (Seber et al., 1996), as well as active oceanic subduction (Gutscher et al., 2002). The onset of Alboran extension is thought to be marked by a heating episode and the rapid exhumation of high-metamorphic rocks at the beginning of the Miocene around 20 Ma ago (e.g. Platt et al., 2003). It has been proposed that this major reorganization of regional tectonics was preceded and originated by convective removal, or gravitational collapse of thickened continental lithosphere (Platt and Vissers, 1989), or alternatively by processes related to the evolution of the western Mediterranean subduction system (Jolivet and Faccenna, 2000), such as retreating subduction of a slab of oceanic lithosphere (Lonergan and White, 1997), mantle flow around a narrow slab tongue (Faccenna et al., 2004) or slab break-off or detachment (Zeck, 1996) around 20–25 Ma ago.

In this paper we aim at a more detailed and quantitative description of present-day, regional crustal deformation in Iberia and the Maghreb. We present 86 moment tensor estimates obtained from systematic analysis of small and moderate regional earthquakes for the period 2002 to May 2005. Adding previous solutions for the period 1984 to 2001 (Stich et al., 2003), we assembled a moment tensor database for 147 events altogether. We use these data to better characterize the kinematics and pattern of seismically active faults within the Iberia–Maghreb region, and determine average stress tensors along several sections of the plate boundary zone. We compare seismological observations to recent Global Positioning System (GPS) velocities, derived from the analysis of permanent and non-permanent networks (Serpelloni et al., 2002, 2005, submitted for publication), and their combination with the European Permanent Network (EUREF-EPN; http://epncb.oma.be) velocity solution. This allows us to test the consistency between strain and stress fields and seismicity distribution. We focus our discussion on the Trans-Alboran shear zone (TASZ hereinafter, Bousquet, 1979; Leblanc and Olivier, 1984; De Larouzière et al., 1988; Sanz de Galdeano, 1990), a belt of distributed shear deformation extending from southeastern Spain over the Alboran Sea to the Mediterranean Moroccan margin, which is well represented in our moment tensor catalogue. Compared to a classical transform fault connecting the Northern Algerian and SW-Iberian compressive margins, the TASZ has an inverse, left-lateral sense of shear, and an unexpected oblique (N35°E) orientation, nearly perpendicular to the regional geodetically derived plate convergence. We thus may suspect that this regional-scale structure is closely related to extension in the Alboran region, and that it plays a key role in accommodating regional strain and explaining complex kinematics of the Iberia–Maghreb plate boundary.

2. Regional moment tensor inversion

Earthquakes from the beginning of 2002 to May 2005 are analyzed for this study. We considered candidates for moment tensor inversion earthquakes with local magnitude larger than 3.5 for the Betic–Alboran region and rest of Iberia, and earthquakes larger than 4.0 for peripheral areas with respect to the Ibero–Maghrebian seismic network, such as northern Africa, the eastern Atlantic Ocean and the Pyrenees. We use three-component regional displacement waveforms, including body and surface waves, for time-domain inversion of the first-order, deviatoric seismic moment tensor. The solution is obtained by minimizing, in a least squares sense, the misfit between observed waveforms and a linear combination of fundamental fault Greens functions (Langston et al., 1982). A unit step source time function is assumed, and for events larger than magnitude 6 a generic centroid time delay was introduced into the Greens functions (6 s for the M_W 6.9, 2003 Bourmedes, Algeria and 3 s for the M_W 6.3, 2004 Al Hoceima, Morocco earthquake).

Greens functions are computed with a reflection matrix algorithm (Randall, 1994; Randall et al., 1995). The underlying plane layered earth models approximate average properties of the lithosphere in the study area. Three different models are used for wave propagation either off-shore, within Alpine domains, or within Hercynian domains (Stich et al., 2003), the latter one is also preferred for mixed paths. Waveforms are filtered in an intermediate period pass band in order to achieve an adequate correction of propagation effects, restricting the inversion to wavelengths that average out small-scale lateral heterogeneities, while at the same time preserve a sufficient signal to noise ratio in the waveforms. Commonly selected filter bands are 50 to 20 s period for events with $M_W > 4$, and 35 to 15 s for smaller events. For the smaller events, most useful waveforms correspond to observations at epicentral distances less than 300 km.

Beyond this range, the combined effects of background noise and crustal heterogeneity complicate accurate waveform matching. For the 50 to 20 s period band, our average earth models allows an adequate prediction of propagation effects for most travel paths over the entire region.

Intermediate period moment tensor inversion in a structurally non-uniform environment is potentially unstable, and usually requires manual intervention. We introduce trial-and-error weighting factors for individual traces to compensate noise and potentially inappropriate corrected propagation effects, and obtain more accurate fits between observed and predicted waveforms. Travel times are calibrated for P-waves by aligning observed waveforms and Greens functions at the first arrivals, reducing the influence of location errors and regional-scale lateral velocity variations on phase matches. Since hypocenter depth is often poorly resolved from arrival times at the regional network, we run moment tensor inversion for a set of trial depths (2 km increment for shallow events and 10 km for mantle earthquakes). This allows us to assess possible trade-offs and retrieve the formally best combination of depth and mechanism. Examples of moment tensor inversion results, and corresponding waveform matches for different geographic and tectonic areas, are given in Fig. 2. A more detailed description of the inversion scheme, lithosphere models, regional seismic networks and data processing can be found in Stich et al. (2003).

Numerical solutions for 86 moment tensors from 2002 to May 2005 are given in Table 1. The equivalent force systems connected with the moment tensors are interpreted in terms of shear failure in tectonic earthquakes, obtaining fault angle parameters for the nodal planes of the double couple moment tensor, as well as a percentage of non-double couple remainder (CLVD). CLVD components are below 30% for all but three solutions. For regional intermediate period inversion, this amount of CLVD is plausible to be introduced by background noise, unaccounted propagation effects or epicenter mislocation (Mancilla et al., 2002). Based on the quality of waveform matches, station coverage and stability of the solution, as well as a systematic analysis of variance reduction for alternative faulting solutions, we attribute a good resolution to 69 moment tensor estimates (quality a and b according to the criteria described in Stich et al., 2003). Further 17 solutions are classified as quality c. Those are less well resolved from available regional broad-band waveforms, but are considered useful estimates, and expected to reproduce the general style and orientation of faulting. Complete inversion results, including numerical data and waveform fits, are posted on-line at www.ugr.es/~iag/tensor, and were communicated to the International Seismological Center (ISC, www.isc.ac.uk) and the EMMA source parameter database (Vannucci and Gasperini, 2004).

3. Geometry and kinematics of faulting

These moment tensor estimates significantly increase the amount of solutions for the wider Ibero–Maghreb plate boundary zone, as well as for intraplate regions where no or few focal mechanism data where available previously, providing relevant pieces for the regional seismotectonic puzzle. With solutions for the period 1984 to 2001 (Stich et al., 2003), which were obtained from an identical inversion scheme but for a generally sparser seismic network, we assembled a moment tensor catalogue for 147 earthquakes altogether (Fig. 3). The data set reveals a variety of regionally consistent faulting trends. We will go through these patterns, reporting some characteristics of regional seismicity, and identifying regional subsets of solutions for a subsequent estimation of average stress tensors.

The Algerian Mediterranean margin shows the most homogeneous faulting pattern within the studied region, with nearly all seismic deformation occurring due to shallow thrusting with ~ NNW–SSE oriented shortening direction. Here, moderate to large earthquakes occur with certain frequency, and a wealth of moment tensor estimates is available through the Harvard CMT catalogue (Dziewonski and Woodhouse, 1983), INGV Regional CMT catalogue (Pondrelli et al., 2002) and ETH regional moment tensor catalogue (Braunmiller et al., 2002; Braunmiller and Bernardi, 2005), all giving a predominance of reverse faulting, as well as less frequent, lower magnitude strike-slip mechanisms. Three odd, NW–SE trending vertical dip slip mechanism in our catalogue are interpreted to be an artifact due to

Fig. 2. Four examples of regional moment tensor inversion for small to moderate (M_w 4 to 5) earthquakes with different faulting style and from different regions. Events are identified with the date (year-month-day), with an optional additional letter B marking that it is the second event in temporal order in our catalogue for that day. For each solution, a location map with stations, moment tensor solution and magnitude, the L2-misfit versus depth, and waveform fits are given. In the misfit- vs.-depth panels, the moment tensor solutions for each trial depth are plotted, with a superscript number indicating the percentage of CLVD component at that depth. Waveform panels compare predicted (dashed lines) and observed (solid lines) intermediate period displacement (in [m]) for 300 s long time windows. Traces are radial, transverse and vertical waveforms from top to bottom. The station name is labeled above each panel.

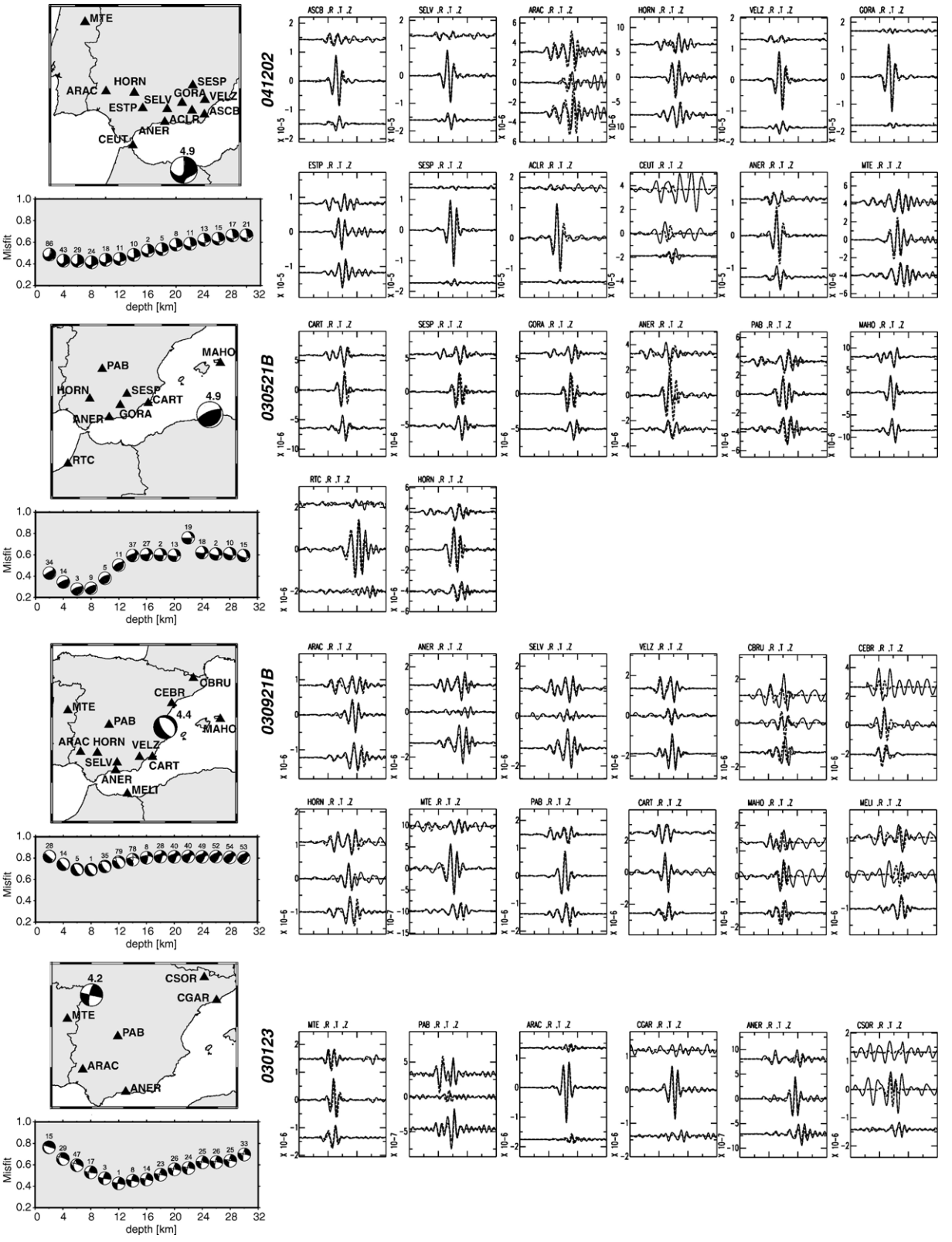
041202
MTE
HORN
SESP
ARAC
GORA
VELZ
SELV
ESTP
ASCB
ACLR
ANER
CEUT
4.9
Misfit
depth [km]
ASCB .R .T .Z
SELV .R .T .Z
ARAC .R .T .Z
HORN .R .T .Z
VELZ .R .T .Z
GORA .R .T .Z
ESTP .R .T .Z
SESP .R .T .Z
ACLR .R .T .Z
CEUT .R .T .Z
ANER .R .T .Z
MTE .R .T .Z
030521B
MAHO
PAB
HORN
SESP
CART
4.9
ANER
GORA
RTC
CART .R .T .Z
SESP .R .T .Z
GORA .R .T .Z
ANER .R .T .Z
PAB .R .T .Z
MAHO .R .T .Z
RTC .R .T .Z
HORN .R .T .Z
030921B
CBRU
CEBR
MTE
4.4
PAB
MAHO
ARAC HORN
VELZ
SELV
CART
ANER
MELI
ARAC .R .T .Z
ANER .R .T .Z
SELV .R .T .Z
VELZ .R .T .Z
CBRU .R .T .Z
CEBR .R .T .Z
HORN .R .T .Z
MTE .R .T .Z
PAB .R .T .Z
CART .R .T .Z
MAHO .R .T .Z
MELI .R .T .Z
030123
4.2
CSOR
CGAR
MTE
PAB
ARAC
ANER
MTE .R .T .Z
PAB .R .T .Z
ARAC .R .T .Z
CGAR .R .T .Z
ANER .R .T .Z
CSOR .R .T .Z

Table 1
Numerical results of moment tensor inversion

Date	Time (UT)	Latitude, [°]	Longitude [°]	Z [km]	Moment tensor elements [Nm]					Double couple (strike/dip/rake)	CLVD [%]	M_0 [Nm]	M_W	q
					m_{xx}	m_{yy}	m_{xy}	m_{xz}	m_{yz}					
020328	04:09:23	37.99	−9.36	20	−7.84e+13	−2.00e+14	4.37e+14	−3.52e+14	1.85e+13	255/72/132, 4/46/26	25	6.14e+14	3.8	c
020627	13:29:50	35.63	−4.03	14	−2.08e+14	5.47e+14	2.05e+14	−3.12e+14	1.25e+14	132/55/−143, 19/61/−40	11	6.19e+14	3.8	c
020706	17:24:19	35.63	−3.92	18	−3.22e+14	1.63e+15	7.38e+14	−8.38e+14	4.24e+14	132/52/−135, 11/57/−47	6	1.92e+15	4.2	c
020806	06:16:19	37.90	−1.84	8	−8.95e+15	2.43e+16	1.96e+16	−1.92e+16	1.15e+15	119/68/−140, 11/53/−27	3	3.47e+16	5.0	a
020806	11:55:17	37.90	−1.83	6	3.94e+12	3.97e+14	4.78e+14	−5.95e+14	−1.82e+14	115/73/−122, 0/35/−28	15	8.81e+14	3.9	b
020807	00:43:57	37.85	−1.82	6	−3.02e+13	1.35e+14	9.98e+13	−1.67e+14	−4.19e+13	120/74/−124, 7/37/−27	13	2.34e+14	3.5	b
020807	23:09:08	37.87	−1.84	6	−1.63e+14	7.63e+14	3.47e+14	−7.07e+14	−2.63e+14	130/70/−122, 11/37/−33	15	1.08e+15	4.0	a
020824	10:08:07	36.46	−4.56	70	−6.28e+14	1.89e+14	7.33e+14	−7.09e+14	2.12e+15	96/21/165, 201/85/70	3	2.42e+15	4.2	b
020915	20:54:19	37.16	−5.27	4	−7.51e+14	−8.23e+13	−7.21e+14	−8.96e+14	2.61e+14	273/68/58, 152/38/143	5	1.42e+15	4.1	a
021210	13:51:26	36.19	−7.47	6	−5.98e+15	−1.25e+16	1.00e+16	1.86e+16	−2.63e+16	35/75/90, 217/15/91	7	3.75e+16	5.0	c
021211	20:09:51	43.05	−0.32	4	2.34e+14	5.17e+13	1.32e+13	3.66e+14	4.17e+13	93/18/−93, 276/72/−88	21	4.53e+14	3.7	c
021212	17:59:51	43.02	−0.36	8	3.76e+14	5.47e+14	2.86e+14	−7.67e+14	−5.61e+14	131/69/−97, 329/22/−72	28	1.28e+15	4.0	b
030101	00:55:55	36.13	2.91	2	−1.09e+16	3.33e+15	9.86e+14	−2.11e+16	−1.48e+16	58/16/28, 302/82/105	11	2.76e+16	4.9	c
030112	15:56:35	41.53	−6.00	10	−1.57e+14	1.31e+14	6.02e+14	3.67e+13	−1.28e+14	277/78/−179, 187/89/−11	10	6.34e+14	3.8	b
030123	10:13:18	41.54	−6.01	12	−8.86e+14	8.43e+14	1.91e+15	5.46e+14	1.71e+14	102/88/165, 192/75/2	1	2.17e+15	4.2	a
030124	20:35:00	37.74	−4.70	12	1.95e+15	−1.79e+15	8.73e+14	−3.36e+13	1.85e+14	58/86/−176, 327/86/−3	14	2.08e+15	4.2	a
030215	03:56:33	35.58	−3.83	12	−7.35e+14	8.10e+14	3.75e+14	−3.22e+14	2.41e+14	124/67/−171, 30/81/−23	10	9.50e+14	4.0	c
030218	13:09:35	35.67	−3.55	4	−1.91e+16	1.66e+16	−5.49e+15	1.19e+14	−7.68e+15	56/72/15, 321/76/161	6	2.03e+16	4.8	a
030218	13:59:29	35.67	−3.61	2	−5.71e+14	1.69e+14	−4.71e+14	5.06e+14	−2.60e+14	81/72/49, 331/44/153	2	8.97e+14	3.9	b
030219	00:33:50	35.73	−3.49	4	−9.43e+14	6.43e+14	−2.88e+14	−4.06e+14	−7.29e+14	60/45/14, 320/80/134	2	1.21e+15	4.0	a
030221	11:46:37	35.69	−3.62	4	−1.96e+15	1.79e+15	−3.48e+14	−1.28e+15	−9.38e+14	48/51/0, 138/90/−141	34	2.49e+15	4.2	b
030221	12:06:49	35.69	−3.60	2	−4.37e+14	4.59e+14	1.60e+13	−3.13e+14	−2.90e+14	135/89/−136, 43/46/−1	1	6.19e+14	3.8	b
030222	11:07:45	35.70	−3.55	4	−2.48e+14	2.25e+14	−1.85e+14	−2.56e+14	1.39e+14	245/88/44, 153/46/177	3	4.19e+14	3.7	b
030521	18:44:20	36.96	3.63	4	−9.90e+18	−9.23e+17	5.78e+18	−2.37e+19	6.87e+18	52/13/69, 253/77/95	11	2.73e+19	6.9	a
030521	23:23:43	36.92	3.50	6	−1.15e+16	−5.32e+15	9.26e+15	−2.03e+16	6.93e+15	247/71/99, 41/21/65	2	2.77e+16	4.9	a
030522	03:14:03	37.08	3.63	8	−1.52e+16	−1.06e+16	7.96e+15	−2.65e+16	1.57e+16	51/19/83, 238/71/92	23	3.89e+16	5.0	a
030522	11:11:05	37.14	3.85	6	−2.87e+15	4.76e+14	5.34e+14	−7.75e+15	6.29e+14	75/10/80, 265/81/92	13	8.23e+15	4.6	c

Table 1 (*continued*)

Date	Time (UT)	Latitude, [°]	Longitude [°]	Z [km]	Moment tensor elements [Nm]					Double couple (strike/dip/rake)	CLVD [%]	M_0 [Nm]	M_W	q
					m_{xx}	m_{yy}	m_{xy}	m_{xz}	m_{yz}					
030522	13:57:20	37.03	3.93	12	−1.83e+16	−5.73e+15	4.15e+15	−3.37e+16	3.48e+15	70/17/78, 262/74/94	24	4.05e+16	5.0	b
030524	19:21:24	37.04	3.97	6	−7.36e+15	8.72e+14	1.11e+15	−1.74e+16	1.76e+15	80/11/86, 264/79/91	10	1.89e+16	4.8	b
030527	17:11:28	36.94	3.58	10	−1.99e+17	−7.66e+16	1.13e+17	−2.94e+17	4.96e+16	254/69/100, 47/23/65	13	4.03e+17	5.7	a
030528	06:58:37	36.88	3.27	6	−7.85e+15	−5.67e+14	2.79e+15	−1.03e+16	4.45e+14	59/21/67, 264/70/99	1	1.34e+16	4.7	b
030529	02:14:59	36.82	3.36	6	−3.41e+14	3.11e+15	2.55e+16	−4.21e+15	1.92e+16	95/53/−173, 0/84/−36	13	3.23e+16	5.0	b
030718	21:23:15	36.97	−6.57	60	−3.80e+14	1.81e+14	9.54e+14	3.12e+14	1.26e+14	189/70/9, 96/82/160	21	1.06e+15	4.0	b
030720	13:12:05	38.00	0.63	14	−6.48e+13	5.91e+13	1.37e+14	−2.24e+13	3.08e+13	12/85/−12, 103/77/−175	15	1.55e+14	3.4	c
030720	21:09:08	38.95	−0.28	4	8.80e+12	4.79e+13	1.45e+13	−5.48e+13	−8.13e+13	148/76/−96, 351/15/−67	12	1.12e+14	3.3	c
030725	03:37:55	36.90	−5.56	6	−5.54e+13	−1.28e+14	9.15e+13	−3.37e+13	2.20e+13	29/40/82, 219/51/96	6	1.91e+14	3.5	b
030729	05:31:26	35.69	−10.56	60	−9.98e+16	5.73e+16	−3.33e+16	−4.31e+16	5.71e+16	243/72/41, 139/51/157	11	1.17e+17	5.3	a
030910	20:22:47	37.11	−3.79	12	1.80e+14	2.78e+13	1.63e+14	4.16e+14	1.32e+14	289/76/−100, 143/17/−55	22	5.05e+14	3.8	c
030916	11:02:47	39.39	0.01	8	1.17e+13	1.14e+15	8.58e+14	−1.48e+15	−8.59e+14	359/27/−40, 127/73/−111	9	2.23e+15	4.2	b
030916	20:19:48	39.39	0.01	8	1.92e+13	9.10e+13	9.59e+13	6.11e+13	−6.38e+13	175/58/−47, 296/51/−137	15	1.66e+14	3.4	c
030921	09:58:55	39.39	0.04	8	3.40e+14	1.74e+15	1.58e+15	−2.28e+15	−1.20e+15	352/28/−45, 125/70/−110	13	3.59e+15	4.3	b
030921	10:34:16	39.41	0.01	8	1.50e+15	2.39e+15	1.91e+15	−1.42e+15	−2.65e+15	148/64/−84, 315/27/−101	1	4.92e+15	4.4	a
031030	01:12:03	37.76	−2.07	4	−1.23e+14	−6.86e+13	8.10e+13	−8.57e+13	8.36e+13	58/29/97, 230/61/86	10	2.22e+14	3.5	b
031116	21:36:12	37.53	−2.65	8	1.40e+14	1.31e+15	2.28e+14	−2.48e+14	−1.42e+14	161/49/−100, 357/42/−77	17	1.43e+15	4.1	b
040110	18:38:15	36.94	3.43	6	−3.92e+15	6.01e+15	5.79e+15	−1.66e+16	−9.30e+15	119/86/−111, 19/21/−10	13	2.06e+16	4.8	c
040224	02:27:46	35.14	−4.00	14	−9.73e+17	1.53e+18	2.31e+18	−9.39e+17	5.25e+17	11/72/−17, 107/73/−161	4	2.88e+18	6.3	b
040224	11:04:44	35.17	−4.08	16	−1.48e+15	2.64e+15	1.55e+15	−1.75e+15	3.39e+14	123/67/−148, 19/61/−26	13	3.29e+15	4.3	b
040224	16:42:12	35.05	−4.08	10	−6.11e+14	7.31e+14	1.39e+15	−6.74e+14	6.89e+13	11/68/−7, 104/83/−157	7	1.69e+15	4.1	a
040224	18:53:02	35.07	−3.91	10	−3.56e+14	4.75e+14	8.39e+14	−3.12e+14	7.72e+14	106/49/−173, 12/85/−40	13	1.26e+15	4.0	b
040224	20:37:02	35.11	−3.95	16	−4.89e+13	3.03e+14	9.80e+14	−2.08e+14	1.97e+14	97/74/−165, 3/76/−15	25	1.06e+15	4.0	b
040225	05:21:14	35.12	−3.93	14	1.50e+14	3.70e+14	4.39e+15	−1.69e+15	1.10e+14	0/69/−4, 92/86/−158	14	4.73e+15	4.4	a
040225	12:44:54	35.05	−3.86	10	−3.13e+16	3.47e+16	5.45e+16	−2.14e+16	1.58e+16	108/73/−167, 14/77/−16	18	6.91e+16	5.2	a
040225	16:33:28	35.17	−3.94	10	−6.52e+14	8.57e+14	6.72e+14	−3.70e+14	1.38e+14	117/73/−162, 22/73/−16	5	1.10e+15	4.0	b
040226	12:07:03	35.19	−4.06	16	−1.04e+16	1.15e+16	2.05e+16	−7.11e+15	2.62e+15	13/75/−9, 105/80/−165	9	2.45e+16	4.9	a

(continued on next page)

Table 1 (*continued*)

Date	Time (UT)	Latitude, [°]	Longitude [°]	Z [km]	Moment tensor elements [Nm]					Double couple (strike/dip/rake)	CLVD [%]	M_0 [Nm]	M_W	q
					m_{xx}	m_{yy}	m_{xy}	m_{xz}	m_{yz}					
040227	00:59:00	35.13	−3.99	14	−1.16e+15	1.41e+15	3.51e+15	−9.16e+14	1.21e+15	102/71/−170, 8/81/−19	11	4.04e+15	4.4	a
040227	03:12:36	35.13	−3.96	12	−8.78e+14	1.40e+15	2.76e+15	−8.40e+14	−1.83e+13	10/73/−5, 102/84/−163	23	3.13e+15	4.3	a
040227	16:50:42	35.18	−3.92	14	−2.92e+15	3.99e+15	4.78e+15	−1.72e+15	3.05e+14	110/80/−163, 16/74/−10	17	6.22e+15	4.5	b
040228	16:29:25	35.02	−4.01	4	−1.48e+15	6.02e+14	8.13e+14	−1.61e+15	−7.97e+14	36/35/23, 287/77/123	2	2.36e+15	4.2	a
040302	20:36:26	35.14	−3.87	12	−1.46e+15	2.57e+15	3.10e+15	−7.01e+14	1.36e+15	109/65/−167, 13/79/−25	28	4.12e+15	4.4	b
040307	06:37:52	35.06	−4.01	22	−2.51e+15	4.48e+15	3.64e+16	−6.21e+15	5.44e+15	93/81/−171, 2/81/−8	0	3.76e+16	5.0	b
040310	04:22:18	34.91	−4.08	6	1.32e+14	4.77e+14	7.17e+14	−1.93e+14	6.58e+14	354/68/−50, 109/44/−148	2	1.14e+15	4.0	b
040312	17:21:51	34.92	−4.05	6	1.89e+15	1.72e+16	1.05e+16	−5.55e+15	3.55e+15	352/49/−62, 134/47/−118	10	2.20e+16	4.9	a
040315	12:39:13	35.11	−4.20	12	−1.47e+14	5.12e+14	4.25e+14	−2.52e+14	2.48e+14	119/54/−148, 9/65/−39	9	7.17e+14	3.9	b
040320	09:37:26	35.00	−4.15	10	−3.53e+15	5.45e+15	3.93e+15	−2.39e+15	3.12e+15	119/56/−164, 20/77/−34	6	7.34e+15	4.5	a
040324	00:59:10	36.01	−8.71	50	−1.93e+14	3.90e+14	3.31e+14	3.86e+14	8.51e+13	297/76/224, 194/47/−18	1	6.17e+14	3.8	b
040401	00:25:35	35.09	−4.09	8	−9.43e+14	6.08e+14	7.13e+14	−6.48e+14	−3.89e+14	28/53/14, 289/79/142	10	1.33e+15	4.0	b
040406	01:53:09	35.05	−4.11	6	−1.40e+15	6.86e+14	7.79e+14	−9.96e+14	1.61e+15	110/33/160, 216/79/59	9	2.38e+15	4.2	b
040416	19:23:25	37.67	−1.38	4	−5.24e+14	5.84e+14	−3.99e+14	3.10e+14	3.04e+14	335/82/−149, 240/60/−8	20	8.11e+14	3.9	c
040620	22:47:05	34.94	−3.88	6	2.34e+14	1.94e+15	1.66e+15	−7.65e+14	9.85e+14	122/47/−131, 355/57/−54	9	2.93e+15	4.3	b
040710	17:57:16	35.16	−4.07	6	1.25e+12	2.34e+14	2.56e+14	−7.81e+13	1.38e+14	358/62/−46, 115/50/−141	29	3.82e+14	3.7	c
040814	01:55:42	34.87	−3.89	6	7.14e+13	3.34e+14	2.06e+14	−2.62e+14	−4.83e+13	129/60/−115, 352/38/−53	16	5.04e+14	3.8	c
040918	12:52:16	42.77	−1.49	12	5.29e+15	−2.63e+14	2.26e+15	−1.45e+15	−3.44e+15	266/38/230, 133/62/−62	4	6.77e+15	4.5	b
040921	15:48:06	42.34	2.17	8	2.06e+15	1.74e+15	2.70e+15	1.77e+15	−6.85e+14	291/55/241, 156/44/−54	2	4.66e+15	4.4	a
040930	13:09:06	42.86	−1.53	8	1.12e+15	4.77e+12	2.07e+14	−1.94e+14	−1.96e+14	108/51/−79, 272/40/258	2	1.17e+15	4.0	a
041010	08:13:59	35.07	−4.06	22	−2.95e+14	7.43e+14	9.92e+14	−2.04e+14	−2.95e+14	284/85/170, 14/80/6	73	1.24e+15	4.0	c
041202	17:50:42	34.95	−2.96	8	5.84e+14	−3.84e+14	2.03e+16	−3.33e+15	1.92e+16	92/47/183, 0/88/−42	24	2.81e+16	4.9	a
041204	10:30:00	34.99	−3.00	12	3.53e+14	2.36e+15	4.10e+16	−9.00e+15	2.33e+16	93/61/189, 359/82/−28	23	4.81e+16	5.1	a
041209	07:46:02	34.97	−3.08	12	8.29e+13	5.49e+14	5.92e+15	−1.74e+15	2.80e+15	94/66/194, 359/77/−23	23	6.80e+15	4.5	b
041213	14:16:11	36.25	−9.98	8	3.63e+14	−4.52e+15	8.72e+15	−1.58e+16	2.11e+15	257/83/119, 360/30/15	7	1.87e+16	4.8	b
050103	11:34:16	36.68	−7.55	30	−4.50e+14	−1.09e+14	4.07e+14	6.12e+14	−2.02e+13	79/68/111, 212/30/48	9	8.97e+14	3.9	b
050129	07:41:31	37.88	−1.78	10	−1.37e+16	1.48e+16	1.98e+15	−6.40e+15	−3.89e+15	132/85/−153, 40/63/−5	3	1.62e+16	4.8	a
050201	23:53:56	38.02	−1.70	6	−5.21e+12	1.57e+14	1.30e+14	−1.64e+14	−2.42e+13	120/68/−125, 1/40/−35	6	2.61e+14	3.6	b

Table 1 (*continued*)

Date	Time (UT)	Latitude, [°]	Longitude [°]	Z [km]	Moment tensor elements [Nm]					Double couple (strike/dip/rake)	CLVD [%]	M_0 [Nm]	M_W	q
					m_{xx}	m_{yy}	m_{xy}	m_{xz}	m_{yz}					
050203	11:40:33	37.82	−1.79	10	−7.98e+14	1.14e+15	1.46e+15	−1.61e+15	−4.61e+14	110/84/−136, 15/46/−7	6	2.44e+15	4.2	b
050204	01:09:41	37.82	−1.80	6	−2.27e+14	3.91e+14	5.46e+14	−5.68e+14	−1.14e+14	109/82/−136, 11/47/−10	3	8.65e+14	3.9	a
050220	13:26:01	38.02	−6.01	20	−4.27e+14	4.09e+14	−1.70e+12	5.77e+13	−8.52e+13	315/76/177, 46/87/14	3	4.31e+14	3.7	b
050322	09:03:13	34.93	−2.98	6	−1.83e+14	−5.48e+14	2.53e+15	−5.69e+14	3.05e+15	87/37/169, 186/84/53	33	4.06e+15	4.4	b

From left to right, columns give: 1) date in format year-month-day, 2) origin time, 3) latitude and 4) longitude (degrees) of the epicentre (locations are from IAG, IGN or NEIC, depending on the geographic region), 5) depth estimate from moment tensor inversion, defined by the minimum misfit solution obtained for several trial depths, 6) to 10) five independent elements of the cartesian deviatoric moment tensor in [Nm], m_{zz} can be obtained as the sum of m_{xx} and m_{yy} due to the deviatoric constraint for the tensor, 11) fault angle parameters of the two nodal planes for the double-couple component of the moment tensor, given as strike/dip/rake in Aki and Richards (2002) coordinate system, 12) percentage of non-double couple (CLVD) remainder of the moment tensor, 13) total seismic moment [Nm] (Silver and Jordan, 1982), 14) moment magnitude M_0 (Hanks and Kanamori, 1979), and 15) quality assessment according to criteria given in the text and in Stich et al. (2003).

limited azimuthal coverage on the edge of the used station network (only one nodal plane is constrained), since two of them are identified as strike-slip events in other catalogues.

Further to the west, earthquakes are concentrated along the ~ N35°E trending TASZ, marking a seismic zone about 100 km wide and 500 km long (Fig. 4). Relevant recent seismicity, including seismic sequences on the Moroccan margin (Al Hoceima 2004, M_W 6.3), the offshore portion (Alboran Ridge 2003, M_W 4.8) and south-eastern Spain (Murcia 2002 and 2005, M_W 5.0 and 4.8 respectively), contribute to a good definition of the faulting style in the TASZ from 66 mechanisms altogether. Over its entire length, this structure definitely delimits the compressive tectonic regime observed along the Algerian Mediterranean margin. The TASZ is — as the name suggests — characterized by predominately strike-slip faulting, however it shows a significant level of heterogeneity on a local scale. In particular, frequent normal faulting earthquakes (27% of all moment tensor solutions, M_W up to 4.9) and normal slip components in strike-slip events suggest an average transtensional character of present-day deformation. The tectonic structure of the TASZ is dominated by eight major, ~ 50–150 km long, N50°E trending, left-lateral, strike-slip faults arranged in en echelon pattern. These are, from north to south, the Crevillente fault, the Alhama de Murcia fault, the Palomares fault, the Carboneras fault, the western and eastern bounding faults of the Alboran ridge, and the Jebha and Nekor faults that cut through the Moroccan Mediterranean margin (Fig. 4). Left-lateral slip is preferred for solutions associated to the main fault traces and related synthetic tectonic structures.

Partly, current seismicity in the TASZ can be associated to principal faults, for example along the Palomares fault, or at the Alboran ridge, where several shallow (2 to 4 km) strike-slip moment tensor mechanisms (e.g. 030218A, 030221A) indicate left-lateral motion along the main boundary fault system (~ N55°E, Comas et al., 1999). On the other hand, along several of the main fault traces the instrumental and historical seismicity is low. For the Carboneras fault, for example, the late Quaternary (100 ka to present) lateral slip rate at the main fault strand was estimated to be below 0.1 mm/yr (Bell et al., 1997). Along those portions of the TASZ, relevant seismic activity occurs off the main fault traces and deformation seems to be accommodated mainly at smaller scale, secondary faults. The diffuse pattern of strain release, potential fault interactions and local stress transfer may introduce complexity of deformation at local scale, and moment tensor solutions for small and moderate events in the area show a wide variety of faulting style between pure normal faulting (e.g. 020204) and pure reverse faulting (e.g. 000802). Also the minor faults within the TASZ may generate significant seismic hazard: At the Moroccan margin, a dense network of secondary faults between the Nekor and Jebha fault traces is responsible for a M_W 6.0 earthquake in 1994 (Calvert et al., 1997) and a M_W 6.3 earthquake in 2004 (Stich et al., 2005a).

In the central parts of the Betic mountain range, moment tensor mechanisms show predominately normal faulting, and seismicity is mostly related to the formation of Neogene–Quaternary intramountain basins (e.g. Galindo-Zaldívar et al., 1999). Pure normal faulting and nearly N–S striking nodal planes were observed for an event associated to the Guadix–Baza

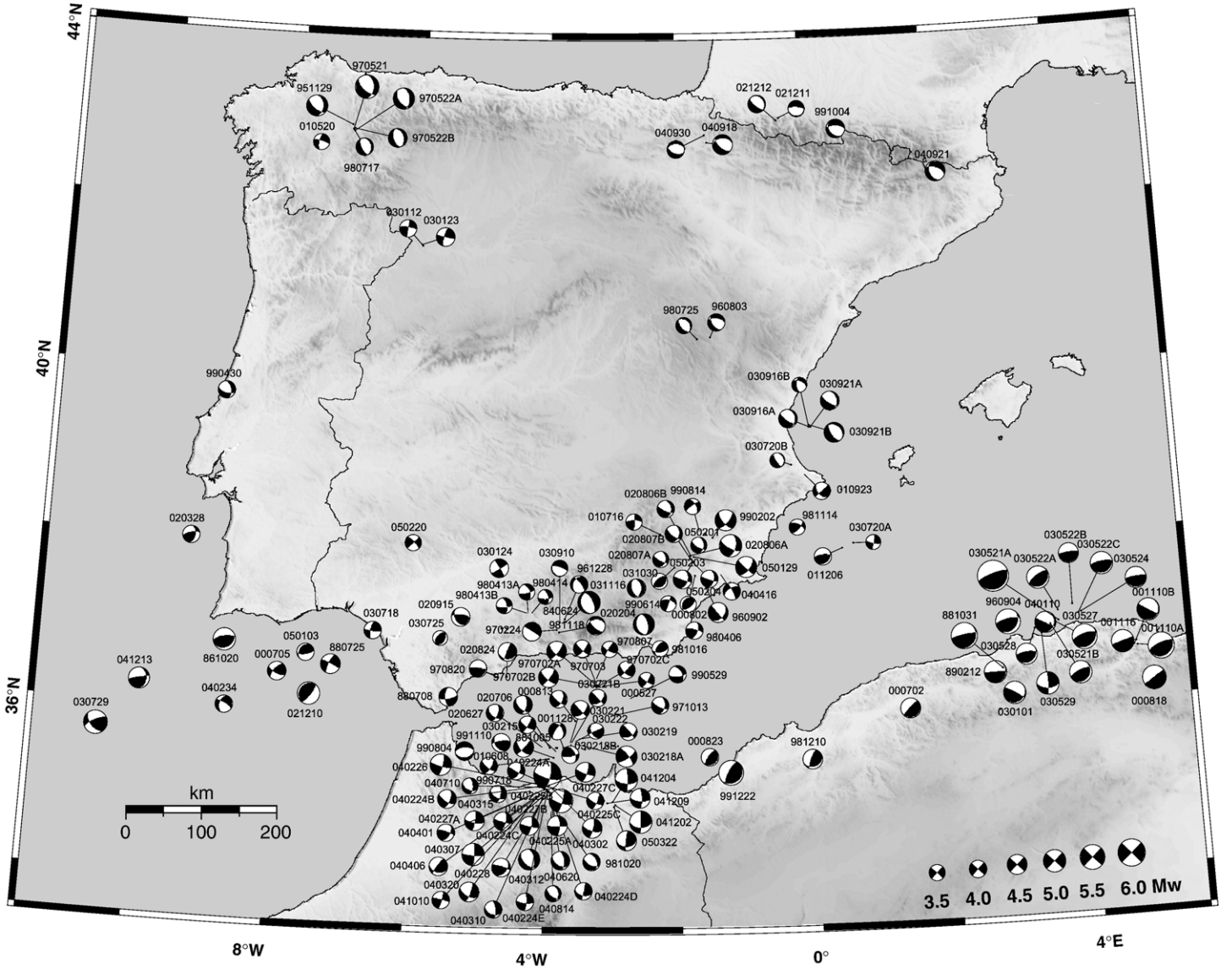

Fig. 3. Geographical representation of the moment tensor catalogue, giving the double-couple components of tensors in equal area, lower hemisphere projection. At each mechanism, an event identification giving the date (year-month-day) is labeled for comparison with Table 1 here, and Table 1 in Stich et al. (2003). Additional capital letters A–E refer to the temporal order of several catalogue solutions for the same day.

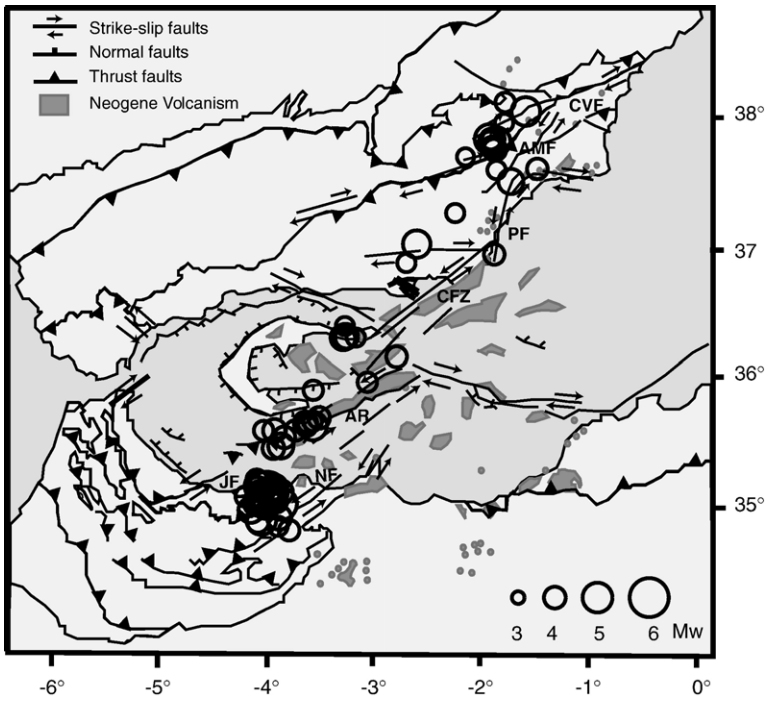

Fig. 4. Map of major strike-slip faults of the TASZ (CVF: Crevillente fault, AMF: Alhama de Murcia fault, PF: Palomares fault, CFZ Carboneras fault, AR: Alboran ridge, JF: Jebha fault, NF Nekor fault) and a selection of related neotectonic elements in the Betic–Alboran–Rif region (redrawn from Lonergan and White, 1997; Comas et al., 1999; Faccenna et al., 2004; Gràcia et al., 2005). Miocene and younger volcanism is indicated in dark grey. Events from the moment tensor catalogue associated to the TASZ are given as black circles.

(031116) basin. Normal faulting mechanisms in and around the Granada basin (37°N, 4°W) show average NE–SW tensional axes and ~ NW–SE striking nodal planes, in agreement with the local trend of normal faults as the dominant neotectonic structures (Morales et al., 1990).

At the SW-Iberian continental margin, earthquakes show reverse or strike-slip faulting with mostly NW–SE to NNW–SSE orientation of pressure axes. Seismicity at the passive continental margin is mostly linked to the tectonic inversion of Mesozoic rifting structures (Zitellini et al., 2004). Seismic catalogues include events at sub-crustal depths down to 60 km in late Jurassic oceanic lithosphere and down to 100 km in the adjacent continental domain, indicating brittle rheology of the uppermost mantle at the ocean continent transition. Four moment tensor estimates in this catalogue have centroid depths greater than 30 km. For this catalogue, as well as for previous source estimates (compilation in Stich et al., 2005b), deformation style and pressure axes orientation are essentially the same for crustal and upper mantle earthquakes, suggesting that mechanical coupling does exist between both domains.

While sub-crustal earthquakes west of the Gibraltar arc resemble crustal deformation and show a diffuse spatial distribution, a different pattern is observed east of the Gibraltar arc. Beneath the Alboran Sea and in southernmost Spain, intermediate deep shocks are concentrated at 4.5°W, between 40 km and 120 km depth within a zone trending southward from the Spanish coast into the Alboran Sea (Seber et al., 1996; Buforn et al., 1997; Morales et al., 1997). Moment tensor solutions for three intermediate deep earthquakes (70 km to 110 km, 970820, 991110, 020824) in this catalogue, as well as four solutions from Buforn and Coca (2002), show near vertical dip slip faulting with varying azimuthal orientation, suggesting a dominance of buoyancy forces over lateral tectonic forces at upper mantle depths.

Earthquakes in Spain and Portugal are not restricted to the immediate proximity of the present day plate contact. In the Pyrenees, moment tensor inversion yields normal faulting with ~ NNE–SSW tension axes, perpendicular to the trend of the mountain chain, however local focal mechanism studies give a more complex seismotectonic picture (e.g. Rigo et al., 2005). Moment tensor solutions in Teruel (960803, 980725) and near Valencia (030720B, 030916A/B, 030921A/B) show normal faulting with ~ NE–SW tension axes, and can be associated to extensional structures of the Teruel rift and Valencia Trough (Vegas and Banda, 1982). In the western parts of Iberia, moment tensor mechanisms

within the Hercynian Iberian massif and along the W-Portuguese margin show predominately normal and strike-slip faulting style (except for event 020328) with an average NE–SW orientation of *T*-axes. North of 39°N, 18 out of 21 catalogue solutions correspond to normal faulting, suggesting regional scale extension of intraplate Iberia.

4. Regional stress tensor estimates

The slip vector of an earthquake dislocation is an indicator for the local stress conditions at the hypocenter. Based on our observation of distinct, regionally consistent faulting patterns within the Iberia–Maghreb area, we use moment tensor mechanisms to quantify the properties and diversity of tectonic deformation by estimating average stress tensors along four sections of the plate boundary zone (SW-Iberian margin, central Betic range, TASZ and northern Algeria) and in intraplate Iberia (Fig. 5). Given the high density of solutions in the TASZ, we perform separate analyses for the northern (north of N36°) and southern part in order to compare deformation at the Spanish and Moroccan margins. Analysis is based solely on our moment tensor catalogue (Fig. 3), for the sake of involving a relatively homogeneous dataset obtained from uniform processing and evaluation criteria. However, we retain that appropriate merging of different catalogues may be a useful alternative in order to increase the number of solutions for those areas where additional regional moment tensor solutions are available, especially the Atlantic and Algerian sections of the plate contact (e.g. Pondrelli et al., 1999, 2002; Braunmiller and Bernardi, 2005).

We quantify average stress tensors using a grid-search approach (FMSI, Gephart, 1990). The parameter space was explored for potential stress tensor principal axes orientations approximately every $2°\times2°$, and for amplitude ratios R between the intermediate stress σ_2 and the maximum and minimum stresses ($R=(\sigma_2-\sigma_1)/(\sigma_3-\sigma_1)$) with increments of 0.02. For each tested stress tensor, the misfit of an individual moment tensor focal

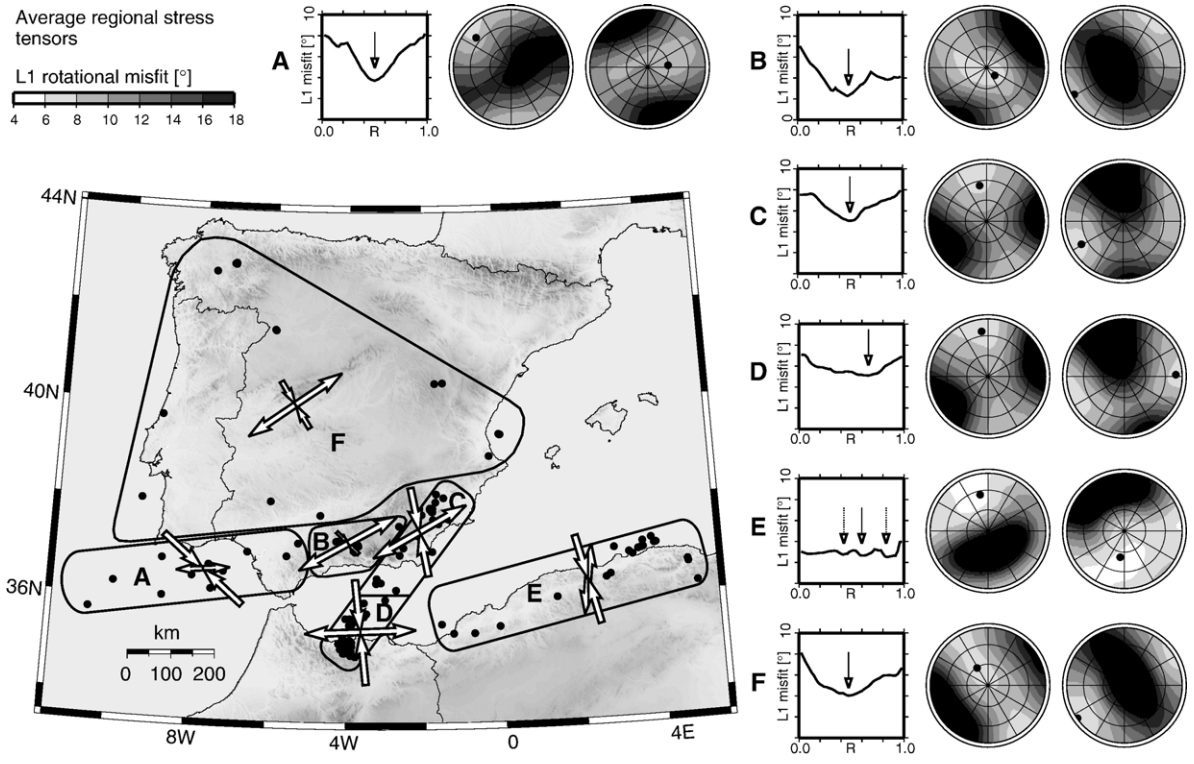

Fig. 5. Regional average stress tensors. The regionalization (map) reflects geotectonic domains and the distribution of seismicity and predominant faulting style over the Iberia–Maghreb region. Epicenters of included moment tensor faulting solutions (124 events out of 147 of the entire catalogue) are plotted as black dots. Irregular geometry of the southern bound of intraplate Iberia (F) partly follows the northern limit of the Betic range. For each stress tensor grid-search we report the relationship of the shape factor R and minimum L1 rotational misfit (left panel), as well as L1 misfit versus $\sigma1$ and versus $\sigma3$ (middle and right panel, lower hemisphere equal area projection of azimuth and plunge) for the formally best R-value. As exception, $\sigma1$ and $\sigma3$ panels for northern Algeria (E) are shown and interpreted for a regional minimum of R (0.60) since R-values are not well resolved from this set of very homogeneous solutions, and the global minimum gives an unexpected high value (0.84). In the map, the projections onto the horizontal plane of $\sigma1$ axes (arrows pointing inward) and $\sigma3$ axes (arrows pointing outward) are given (length proportional to cosine of plunge).

mechanism is defined as the minimum rotation that is necessary to reconcile the stress tensor with the observed slip vector direction on either nodal plane (Gephart, 1990). The misfit of an individual tested stress tensor is expressed as the L1-norm of rotations for the entire set of focal mechanisms involved, with the globally best tensor minimizing this norm. The L1-misfit surfaces (Fig. 5) indicate a relatively good resolution of the stress tensor orientation from focal mechanism populations for the SW-Iberian margin, Betic range and TASZ, while estimates for northern Algeria and intraplate Iberia show larger ambiguities owing to the more homogeneous sets of focal mechanisms involved (c.f. McKenzie, 1969). The inferred average stress tensors (Table 2) are consistent with our previous qualitative assessment of deformation style:

(A) The SW-Iberian margin shows a transpressive stress field, with subhorizontal NW–SE (N310°E) compression and minor E–W extension. The largest principal stress σ_1 is perpendicular to the major neotectonic lineaments (Fig. 1), and sub-parallel to the regional NNW–SSE direction of plate convergence (Serpelloni et al., submitted for publication; a more detailed description of plate kinematics and regional GPS velocity vectors is given in the following section). Uncertainties are associated to the northern limit of the transpressive regime along the W-Iberian margin, where mechanism 020328 shows similar style and orientation of faulting, but was assigned to intraplate Iberia (region F) for geographical affinity. Also a large, M_W 6.0 earthquake in central Western Portugal in 1909 is linked to reverse faulting (Stich et al., 2005c), and GPS observations suggest minor convergence between southern and central Western Portugal (see following section), however a longer observation period will be necessary to resolve adequately the small relative motion.

(B) Intramountain basins in the Betic range are characterized by an extensional stress field, with near-vertical σ_1 axis and near-horizontal σ_3 axis. Present day extension is along ~ N240°E, parallel to the inferred ENE–WSW stretching direction for Alboran rifting during the Miocene (Faccenna et al., 2004).

(C) Seismicity in the northern portion of the TASZ, at the Spanish margin and in the northern Alboran Sea, is consistent with an average transtensional stress field (i.e. a predominately strike-slip regime with the tension axes plunging slightly shallower than the pressure axes) with nearly N–S average compression and ~ N240°E extension. The orientation of extension is parallel to the value for the central Betics and to the direction of Alboran stretching. The largest principal stresses σ_1 at ~ N350°E show a significant clockwise rotation of ~ 45° compared to the regional convergence direction. The transtensional deformation style reflects the current predominance of mechanisms with normal slip component. Reverse slip mechanisms make only a minor contribution to fault zone kinematics during the period represented in our moment tensor catalogue (9% of the solutions, M_W up to 4.2), but their relevance for the long-term, average movement of the TASZ is confirmed by previous geological field works, revealing reverse components of slip, and large ($M_W > 6$) associated paleoearthquakes, along several principal structures, e.g. at the Alhama de Murcia fault (Silva et al., 1993; Martínez-Díaz, 2002; Masana et al., 2004, 2005).

(D) The southern portion of the TASZ, with the Moroccan margin and the southern Alboran Sea, shows a strike slip to transtensional stress field, similar to the one observed in the northern part. Compression is oriented ~ N350°E, again showing a rotation of ~ 45° compared to the plate convergence direction, and extension nearly perpendicular at ~ E–W. Though the inversion is dominated by the 2004 Al Hoceima sequence, contributing 25 of 40 focal mechanisms, the

Table 2
Regional average stress tensors (compare Fig. 5)

Region	Events	Misfit	R	σ_1 (str/pl)	σ_2 (str/pl)	σ_3 (str/pl)	Tectonic regime
SW-Iberian margin	11	3.8°	0.50	310°/22°	212°/19°	85°/61°	RF–SS, transpression, NW–SE shortening
Central Betic range	9	2.4°	0.48	134°/74°	333°/15°	241°/4°	NF, ENE–WSW extension
TASZ nord	26	5.1°	0.50	349°/37°	129°/54°	241°/19°	SS–NF, transtension, N–S shortening, ENE–WSW extension
TASZ south	40	5.1°	0.66	354°/22°	205°/65°	88°/12°	SS–NF, transtension, N–S shortening, E–W extension
N-Algerian margin	19	2.7°	0.84	348°/36°	86°/10°	189°/52°	RF–SS, NNW–SSE shortening (see text)
Central Iberia	19	3.9°	0.48	328°/61°	144°/30°	235°/1°	NF–SS, NE–SW extension

From left to right, columns give: 1) region, 2) number of faulting solutions used, 3) global minimum of L1 rotational misfit, 4) shape factor R, 5) to 7) principal axes of the average stress tensor (trend/ plunge), and 8) a qualitative description of the stress field, including the tectonic regime (NF, normal faulting, RF, reverse faulting, SS, strike-slip faulting) and related deformation (e.g. extension/compression).

inferred orientation of σ_1 is notably different from the average NNW azimuth of *P*-axes for Al-Hoceima earthquakes (Stich et al., 2005a) and is consistent with the observed left-lateral dislocations both at the N55°E principal faults at the Alboran Ridge, and at the N10°E active strike-slip faults in the Al Hoceima area.

(E) For northern Algeria, the stress tensor is only weakly constrained due to a predominance of similar, reverse faulting focal mechanisms with sub-parallel nodal plane orientations. We fixed the value of *R* at a local minimum of the initial inversion (0.60) since *R* is essentially unresolved, and the global minimum gives an unexpected high value (0.84). The resulting σ_1 and σ_3 misfit distributions resemble the compressive and extensional quadrants of the dominant NNW-ward thrust faulting mechanisms, and principal axes orientations are closely related to those of the strain tensor in this case. We attribute a compressive stress field (horizontal σ_1 at 350°E) to this region. As in the TASZ, the principal compressive stress shows a clockwise rotation compared to the regional convergence direction, however this is less well constrained in this case. Moment tensor focal mechanisms itself suggest a anticlockwise rotation of the current shortening direction westward along the N-Algerian margin, which is not represented in the average tensor.

(F) Finally, inversion for intraplate Iberia gives horizontal σ_3 at N235°E, indicating regional NE–SW extension. The underlying dataset merges mechanisms from the Hercynian massif, Iberian Chain and Valencia Trough, however an inversion limited to the Hercynian massif does yield very similar results. L1-misfits are likewise low for near-vertical and near-horizontal, NNW oriented σ_1 axes, suggesting a mixture of extensional and strike-slip regimes in the area. This view is consistent with observed small-scale heterogeneity of the Iberian intraplate stress field (Andeweg et al., 1999; Herraiz et al., 2000; Cloetingh et al., 2002), affecting seismicity and earthquake focal mechanisms directly.

5. GPS observations around the westernmost Mediterranean

Surface velocities obtained from global continuous GPS (CGPS) tracking networks (e.g., the IGS network; http://igscb.jpl.nasa.gov) provide fundamental kinematic boundary conditions for the large scale Africa–Eurasia plate convergence, allowing for comparisons with geological plate models (DeMets et al., 1994; Sella et al., 2002; McClusky et al., 2003; Calais et al., 2003). Regional and local GPS observations, either from continuous or discontinuous GPS (DGPS) networks, typically evidence some inconsistencies and deviations from the continental scale rigid plate motions. Once co- and post-seismic signals are removed, this data represent the regional distribution of inter-seismic strain accumulation, and can be interpreted in terms of block motions and fault kinematics (e.g., McClusky et al., 2000; Meade et al., 2002; McClusky et al., 2003; Nocquet and Calais, 2003; Battaglia et al., 2004). While the large number of GPS data available in the eastern Mediterranean significantly improved our understanding of its present-day kinematics and allowed developing models for crustal deformation (McClusky et al., 2000; Mantovani et al., 2001; Armijo et al., 2003; McClusky et al., 2003; Nyst and Thatcher, 2003), the picture is less clear in the western Mediterranean, mostly due to the significantly lower number of GPS stations available. In this study, velocities obtained from the analysis of CGPS and DGPS networks have been combined with publicly available EUREF-EPN velocities in Spain and Portugal, to obtain an enhanced velocity field for the westernmost Mediterranean region.

We analyzed the 1998–2005 observations of a subset of EUREF-EPN (http://epncb.oma.be) and Italian Space Agency (ASI; http://geodaf.mt.asi.it) CGPS stations, together with data from CGPS stations operating in Morocco and Egypt, installed by the Massachusetts Institute of Technology (data available through the UNAVCO archive, http://www.unavco.org). We also include DGPS data collected at two sites in northern Algeria, which have been repeatedly surveyed in the frame of the TYRGEONET project (see Serpelloni et al., 2002 and references therein). The data set has been analyzed using the GAMIT/GLOBK and QOCA software (Dong et al., 2002; King and Bock, 2004; Herring, 2004) following standard procedures for regional networks in a three step approach (Dong et al., 1998; McClusky et al., 2000). The GPS solution is realized in the ITRF2000 global reference frame (Altamini et al., 2002), and velocity uncertainties have been computed adopting a model that accounts for both white and coloured noise (Mao et al., 1999; Dixon et al., 2000), although this approach is expected to provide over conservative uncertainties (e.g., Mao et al., 1999). More information about GPS data and networks, GPS data processing and post-processing are provided in Serpelloni et al. (2005, in press), to which we refer for further details. To include additional EUREF-EPN

stations in Iberia, we use the published ITRF2000 velocities (http://epncb.oma.be/_dataproducts/time-series/series_sp.html), obtained from a rigorous analysis of their position time series. The associated formal uncertainties have been rescaled following Caporali (2003), to account for unmodeled error sources. In order to test for possible differences in the realization of the two global frames (i.e., due to the different observation time spans involved, different reference stations and geographical coverage of the networks), we compared the two solutions through a seven parameter Helmert transformation, using our solution as the reference one. The differences observed among the common stations are of the order of few tens of mm/yr, and no systematic bias has been detected, allowing for a rigorous combination of the data-sets.

During the observation time-span, no significant earthquakes occurred at distances from the GPS stations considered to cause co-seismic offsets (the observation period at the DGPS station ALGE in N-Algeria, with 5 surveys between 1995–1999, does not contain the co-seismic effects of the nearby M_W 6.9 earthquake in 2003). For this reason the combined velocity field can be taken as representative of longer-term displacements and can be compared with the plate convergence rates predicted by an Africa–Eurasia geodetically derived plate model (Serpelloni et al., submitted for publication). Discrepancy between the Africa–Eurasia convergence rates and directions predicted by the Nuvel-1A model and the geodetically derived models is a well known feature (e.g., Sella et al., 2002; Calais et al., 2003; Kreemer et al., 2003; McClusky et al., 2003; D'Agostino and Selvaggi, 2004). Calais et al. (2003) interpreted this observation as possible changes in last 3 Ma Africa–Eurasia relative motion, related to effect of the ongoing continent–continent collision. All recent studies show that the geodetic models predict convergence rates that are slower and ~ 30° counter-clockwise rotated, in the western Mediterranean, with respect to predictions by the geological Nuvel-1A model. Despite some differences among available geodetic estimates for the Africa (Nubia)–Eurasia relative rotation pole, apparently due to the different data-sets involved and due to the fact that the Nubian plate is still significantly less constrained

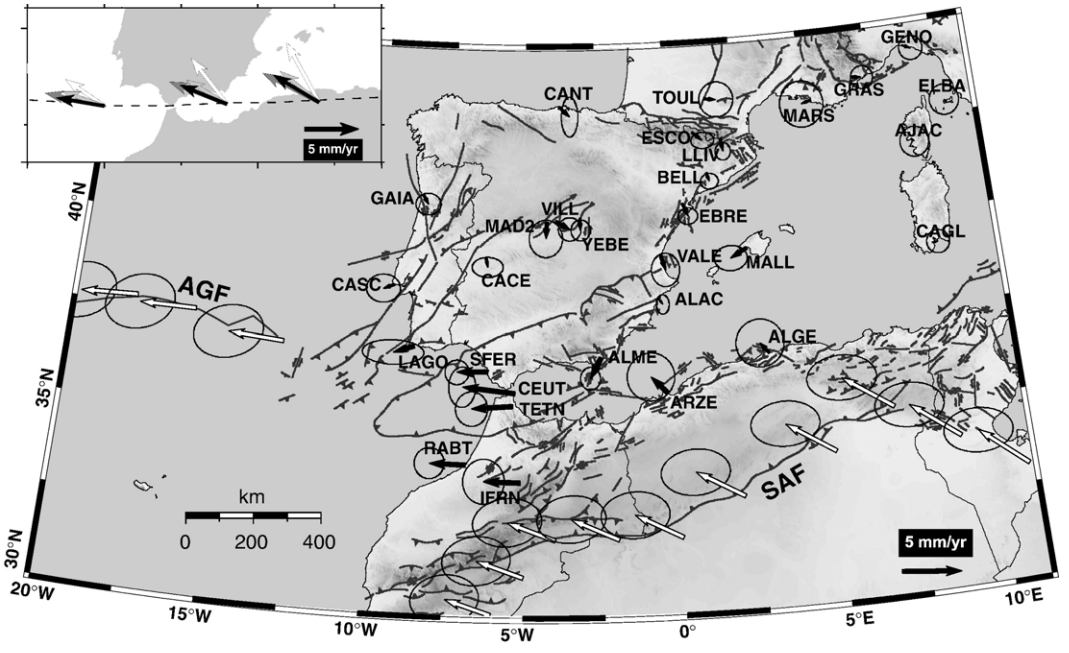

Fig. 6. Combined GPS velocity field around the westernmost Mediterranean. Black arrows give motion (mm/yr) according to Table 3, relative to the stable European reference frame in Serpelloni et al. (submitted for publication). Ellipses show 95% confidence limits. White arrows at the South Atlas boundary fault (SAF) and the Azores Gibraltar fracture zone (AGF) indicate the motion predicted by the Nubia–Eurasia rotation pole (Serpelloni et al., submitted for publication). Most relevant shortening occurs in northern Algeria, with relatively small motion observed at the coast. A minor southward motion of the Iberian Peninsula is apparent. The largest observed GPS velocities indicate westward expulsion of the Gibraltar Arc, and corresponding extension in the Alboran region, see text. The upper left inset displays velocities predicted by geological (Nuvel-1A; white arrows) and geodetic Africa–Eurasia relative rotation poles. Black arrows from Serpelloni et al. (submitted for publication); dark grey arrows from Sella et al. (2002); light grey arrows from McClusky et al. (2003).

than the Eurasian plate, differences in the predicted convergence rates and orientations are rather small in our study area (see upper left inset in Fig. 6).

Fig. 6 shows the combined velocity field (with 95% confidence error ellipses) given with respect to the Eurasian fixed frame computed by Serpelloni et al. (submitted for publication), located at Lon. −105.66±0.46°E, Lat. 52.92±1.11°N, and rotating at a rate of 0.246±0.001°/Myr. White arrows show the velocity vectors predicted by the Nubia–Eurasia Euler vector (located at Lon. −15.89±2.58°E, Lat. −1.0±2.19°N, and rotating at a rate of 0.068±0.003°/Myr; Serpelloni et al., submitted for publication), and would represent the velocities with respect to Eurasia for points located on the stable, non-deforming Nubian plate (i.e., south of the Saharan Atlas front). Despite the still not particularly dense distribution of stations, compared to the apparent tectonic complexity of the study region, our GPS velocities and predicted displacement rates provide a preliminary kinematic framework for understanding crustal deformation at the seismically active plate boundary. Residual velocities with respect to Eurasia, with one standard deviation uncertainties, are listed in Table 3.

Central Mediterranean stations (i.e. AJAC, CAGL, ELBA) and sites located along the southern France coast (i.e. GRAS, MARS) display no significant motion with respect to Eurasia, suggesting that this region is at present rigidly attached to the Eurasian plate, with small to null residual deformation. Residual GPS velocities along the Algeria coast (i.e., ARZE and ALGE) are low and NW-oriented, evidencing that a large portion of the ongoing Nubia–Eurasia convergence in this sector is accommodated in northern Algeria. Given that earthquakes occur also right at the coast, with offshore slip involved for example in the 2003 M_W 6.9 Bourmedes earthquake (Delouis et al., 2004; Braunmiller and Bernardi, 2005), the observed 1.1±0.8 (ALGE) to 1.9±

Table 3
GPS velocity estimates for stations in the western Mediterranean (compare Fig. 6)

Station	Source	Longitude [°]	Latitude [°]	V_{east} [mm/yr]	V_{nord} [mm/yr]	V_{abs} [mm/yr]	σ_{Veast} [mm/yr]	σ_{Vnord} [mm/yr]
CASC	S	−9.420	38.690	−0.91	−0.37	0.98	0.58	0.48
LAGO	E	−8.670	37.100	−1.72	−0.58	1.82	1.05	0.42
GAIA	E	−8.590	41.110	0.48	−0.84	0.97	0.43	0.37
RABT	S	−6.854	33.998	−3.04	0.09	3.04	0.51	0.53
CACE	E	−6.340	39.480	0.17	−0.81	0.53	0.34	0.50
SFER	S	−6.206	36.464	−2.56	−0.04	2.56	0.41	0.42
TETN	S	−5.363	35.562	−3.45	−0.21	3.46	0.55	0.59
CEUT	E	−5.310	35.900	−4.39	0.55	4.42	0.46	0.69
IFRN	S	−5.108	33.540	−3.07	0.10	3.07	0.71	0.77
MAD2	S	−4.250	40.429	−0.07	−1.39	1.39	0.57	0.64
VILL	S	−3.952	40.444	1.20	−0.66	1.37	0.39	0.40
CANT	E	−3.800	43.470	0.89	−0.84	1.22	0.28	0.68
YEBE	E	−3.090	40.530	0.04	−1.03	1.03	0.33	0.36
ALME	E	−2.460	36.850	−0.92	−1.75	1.98	0.34	0.39
ALAC	E	−0.480	38.340	0.34	−0.48	0.59	0.22	0.33
VALE	E	−0.340	39.480	0.35	−1.22	1.27	0.48	0.57
ARZE	S	−0.313	35.858	−1.33	1.39	1.92	0.81	0.82
EBRE	E	0.490	40.820	0.44	−1.06	1.15	0.33	0.28
ESCO	E	0.980	42.690	0.83	−0.73	1.11	0.39	0.28
BELL	E	1.400	41.600	0.23	−0.73	0.77	0.30	0.27
TOUL	S	1.481	43.561	1.01	−0.14	1.02	0.58	0.60
LLIV	E	1.970	42.480	0.17	−1.09	1.10	0.26	0.30
MALL	E	2.630	39.550	−1.39	−0.76	1.58	0.56	0.43
ALGE	S	3.110	36.738	−0.72	0.89	1.14	0.82	0.81
MARS	S	5.354	43.279	−0.81	−0.24	0.84	0.74	0.79
GRAS	S	6.921	43.755	0.85	−0.10	0.86	0.38	0.39
AJAC	S	8.763	41.928	0.24	−0.23	0.33	0.49	0.51
GENO	S	8.921	44.419	0.67	−0.30	0.73	0.40	0.41
CAGL	S	8.973	39.136	0.49	0.05	0.49	0.39	0.40
ELBA	S	10.211	42.753	−0.16	0.27	0.31	0.50	0.52

From left to right, columns give: 1) station acronym, 2) data source including (E) the EUREF-EPN network solutions (http://epncb.oma.be/_dataproducts/timeseries/series_sp.html), and (S) data from Serpelloni et al., submitted for publication. 3) latitude and 4) longitude of the station, 5) and 6) east and north component of GPS velocity [mm/yr], 7) absolute horizontal GPS velocity [mm/yr], 8) and 9) one standard deviation of east and north velocity components [mm/yr].

0.8 (ARZE) mm/yr movement provide an upper bound to relative motion actually transferred to the Western Mediterranean Sea. In northern and central Iberia, inferred GPS velocities are low, of the order of 1 mm/yr, and close to the statistical errors associated with the presently available observations. However, the consistent S- to SSE-ward direction of GPS velocities may be expected to be significant on a regional scale. This will add to the Algerian–Iberian convergence, as well as predict a minor amount of extension between Iberia and Western Europe, in agreement with the predominately normal faulting moment tensor solutions observed for the Pyrenees. Morocco and southernmost Spain show predominately westward velocities relative to Europe. Rather uniform westward motion of the Gibraltar arc and entire northwestern Morocco occurs at ~ 3 to 3.5 mm/yr, with station CEUT showing slightly larger velocities and different trend that might represent some local loading effect at the waterside location of the site. Further north, SFER and LAGO show consistent but smaller velocities, suggesting that both sites are sensitive to strain accumulation associated to a belt of transpressional seismic deformation along the SW-Iberian margin. Stations ALAC and ALME seem to illustrate activity of the TASZ, with station ALAC near the northern end of the shear zone (in the southeastern block of the Crevillente fault) showing near null residual with respect to Europe, and ALME (in the northwestern block of the Carboneras fault) showing south-west ward motion following left-lateral shear.

To integrate the geodetic data and seismotectonics (i.e. seismicity distribution and moment tensor focal mechanisms), we compare the patterns of co-seismic stress release and inter-seismic strain accumulation, i.e. spatial gradients in the GPS velocity field. Since the number and spatial distribution of GPS stations still do not allow to derive a well constrained continuous horizontal strain-rate field over the entire region, quantitative estimates of geodetic deformation rates were obtained by projecting the horizontal GPS velocities along three

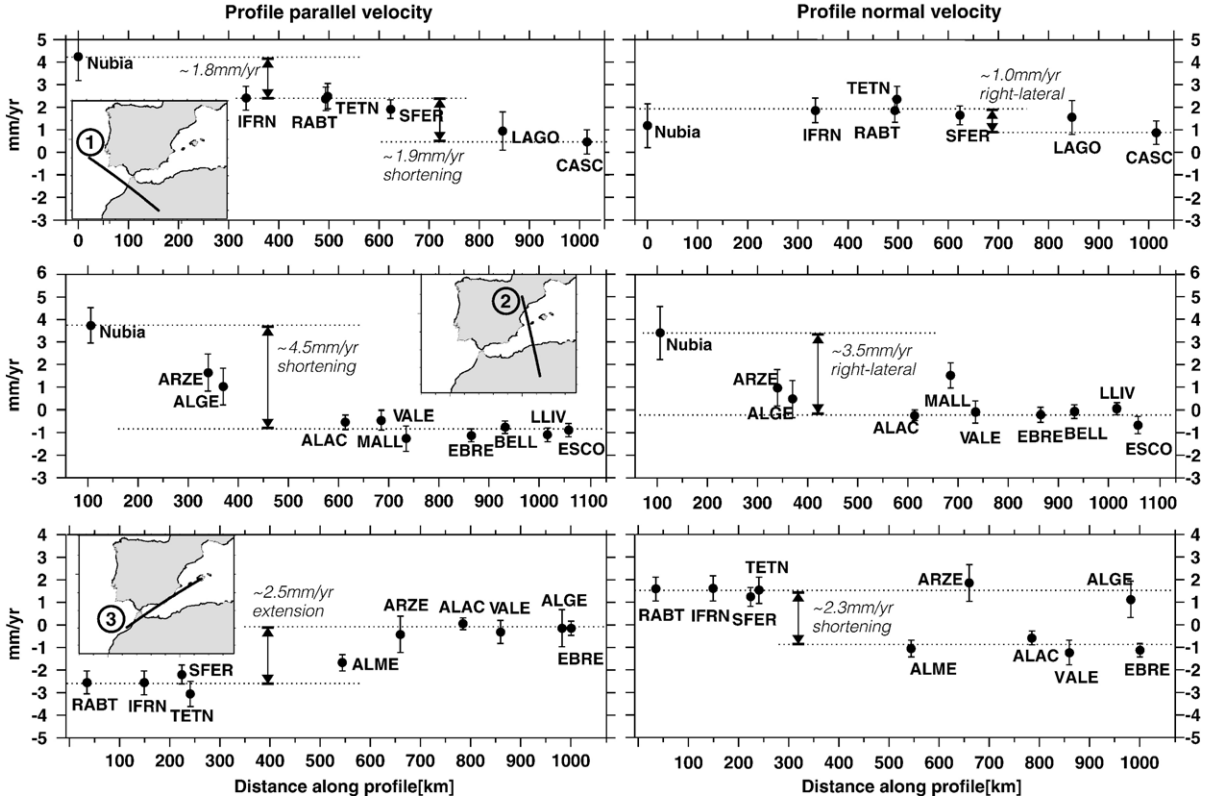

Fig. 7. GPS velocity profiles. Horizontal GPS velocities are projected along 3 profiles parallel to the directions of largest or smallest horizontal stresses, as obtained from regional moment tensor mechanisms (top: SW-Iberian compression, middle: N-Algerian compression, bottom: Betic–Alboran extension, see text). Profile parallel GPS velocity components, and corresponding one standard deviation error bars, are given in the left panels, and the profile normal values in the right panels. Velocities [mm/yr] are given relative to stable Europe. Dashed lines mark the average velocity of groups of stations with relatively uniform motion, or velocity at the end point of the selected profile. Approximate deformation rates between those levels are given.

profiles considered representative for the main active collisional and extensional processes in the region (i.e. constructed along the direction of principal seismic stresses of the corresponding average seismic stress tensors). GPS velocities in northern Morocco and SW-Iberia (profile 1 in Fig. 7) are projected on the N310°E direction of SW-Iberian compression. The near-uniform motion of NW-Morocco implies shortening of ~ 1.8 mm/yr relative to stable Nubia, presumably accommodated in the Middle and High Atlas. The transpressional regime at the SW-Iberian margin corresponds to ~ 1.9 mm/yr shortening between Morocco and station CASC, and ~ 1.0 mm/yr of right-lateral motion. A profile from Algeria to Spain (profile 2 in Fig. 7), along the N350°E direction of largest principal stress axes observed in N-Algeria and the TASZ, indicates ~ 4.5 mm/yr of shortening and ~ 3.5 mm/yr of right lateral motion between intraplate Iberia and stable Nubia. The N-Algerian coastal stations ALGE and ARZE show intermediate values, indicating that ~ 3 mm/yr of shortening and ~ 2.5 mm/yr of right-lateral deformation are accommodated in N-Algeria. Being situated within the seismic belt, these observations are not conclusive for the total amount of deformation at the Algerian margin, and we tentatively propose that ~ 1–2 mm/yr of shortening and a minor right-lateral contribution could be accommodated further to the north. Deformation in the Alboran–Gibraltar region is evaluated along a N240°E profile in direction of smallest principal stresses in the Betics and northern TASZ (profile 3 in Fig. 7). It shows ~ 2.5 mm/yr extension between the Gibraltar arc and easternmost Spain, with stations ALME within the TASZ showing intermediate values. Velocity components perpendicular to the profile provide an alternative projection of shortening values, being somewhat smaller than rates for extension. Superposition of both motions may explain the observed transtensional stress regime in the TASZ, and the left-lateral sense of shear.

6. Discussion

Consideration of seismicity distribution, neotectonics, moment tensor focal mechanisms and GPS velocities together shed some more light on the complex kinematic behavior of the Iberia–Maghreb plate contact than individual datasets could do. We may interpret two ~ ENE–WSW trending, ~ 150 km wide belts of rather focused seismic activity, predominately reverse faulting and geodetic shortening at the SW-Iberian and N-Algerian margin as segments of the obliquely convergent plate boundary. Between these segments, seismicity is more diffuse, but the TASZ stands out from the earthquake distribution as a clearly regional-scale feature. The TASZ has an overall trend of N35°E and displays a left-lateral sense of shear along individual major faults. Together with the compressive margins on either sides, and with the Betic Cordillera, it forms a zed-shaped belt that includes a large portion of the shallow earthquakes at the Iberia–Maghreb plate contact, and coincides with the main gradients in the interpolated GPS velocity field (Fig. 8). Despite this concentration of strain release, we cannot interpret the zed-form straightforwardly as the localized Iberia–Maghreb plate boundary (that is, the Alboran region would have a rigid connection with Nubia), in particular because there is no direct relationship between the geodetic plate convergence direction nearly perpendicular to the TASZ, and the observed transtensional stress regime with ~ N–S oriented σ_1-axis.

Along the Betic portion of the TASZ, left-lateral strike-slip motion since the Tortonian is estimated as 14 km at the Palomares fault (Martínez-Díaz and Hernández-Enrile, 2004) and 17 km at the Carboneras fault (Montenat et al., 1990), indicating average slip rates over geological time scales of about 1–2 mm/yr. This is of the same order as present day deformation derived from GPS measurements. Middle Miocene to Pleistocene calc-alkaline through K-rich volcanism (Duggen et al., 2004) characterize the TASZ as an important zone of weakness along the Iberia–Maghreb plate contact, and magmatic intrusions in the lower crust have been imaged in receiver function studies (Julià et al., 2005). Offshore, the shear zone cuts highly extended continental crust with 12 to 15 km thickness (Torné et al., 2000; Gràcia et al., 2005). At the Moroccan margin, the geometry of neotectonic structures suggest some continuity of the TASZ into the Middle Atlas mountains (Frizon de Lamotte et al., 1991), fading into a more compressive regime, with only a smaller remainder of left lateral shear, and 1–2 mm/yr of shortening observed at the Middle and High Atlas (Gomez et al., 2000; Arboleya et al., 2004, and GPS strain rates presented in this work). To the west, significant left-lateral shear in the Alboran Basin is apparently limited by a change in crustal architecture and rheology around 4°W, coincident with a change in the patterns of free air gravity, heat flow and depth distribution of earthquakes (Andeweg and Cloetingh, 2001).

At about 4.5°W, recycling of lithosphere into the mantle is evidenced by the occurrence of upper mantle earthquakes beneath the Alboran Basin. According to P-wave tomographic images and gravity modeling, most intermediate deep earthquakes in the Alboran Basin seem to be related to low velocity (Serrano et al., 1998; Calvert

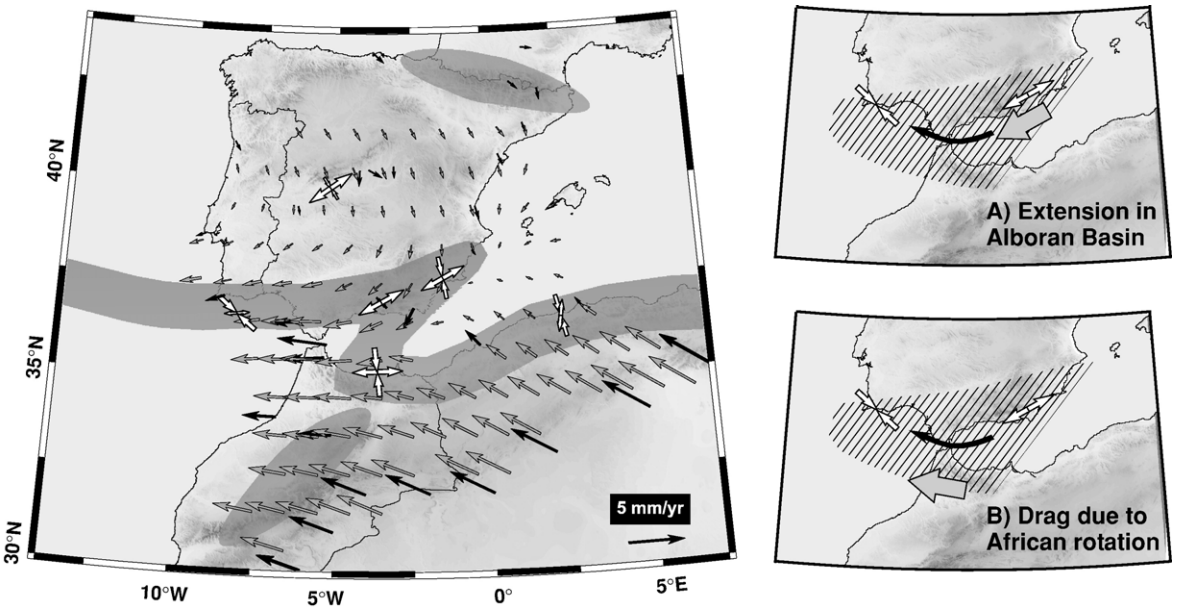

Fig. 8. Summary and schematic interpretation of results. On the left, predicted and observed GPS velocities (black arrows), stress tensor estimates (white arrows) and belts of localized earthquake activity (grey) are shown. Grey arrows display the continuous velocity field obtained by interpolating the GPS velocities over a regular 1° × 1° grid, adopting a damped least-squares algorithm (Shen et al., 1996). A rotation of stress and velocity trajectories over the Betic–Alboran–Gibraltar region is apparent (remind that stress is physically tied to spatial gradients in the velocity field). On the right, two cartoons illustrate possible driving mechanisms for differential motion (black arrow) and internal deformation (white arrows) of the Betic–Alboran–Gibraltar region: A) active extension in the Alboran Sea, pushing the region from the ENE (thick grey arrow), and B) westward drag (grey arrow) due to the torque of Nubian rigid rotation and the relative motion of Morocco, applied to the southern edge of the region.

et al., 2000), low density (Morales et al., 1999) anomalies in the upper mantle, suggesting a relationship of seismicity to sunk continental lithosphere (including a portion of low-density crustal material). Considering regional deformation style, we can term this process as delamination if it propagates in an ~ E–W direction parallel to extension, and as continental subduction if it propagates ~ N–S, parallel to the shortening direction. Delamination offers an integral explanation for both seismicity and regional extension (Mezcua and Rueda, 1997), but hypocenter locations suggest diffuse basin-ward dip of intermediate deep seismicity under the northern and southern margins of the Alboran basin (Seber et al., 1996; Morales et al., 1999), consistent with the expected pattern for subduction. More detailed imaging of uppermost mantle structure may resolve this point in the future.

An alternative geodynamic scenario postulates active eastward subduction of a narrow slab of oceanic lithosphere beneath the Arc of Gibraltar (Gutscher et al., 2002). The corresponding subduction interface is not represented in instrumental seismicity, but it is has been proposed as a possible source of the great 1755 Lisbon earthquake, being currently locked (Thiebot and Gutscher, in press). However, we found that this model is not supported by available GPS observations: While the present-day westward motion in the presumed overriding arc (SFER, CEUT, TETN) is about 2.6 to 4.4 mm/yr relative to stable Europe (one magnitude less than typical subduction velocities), the differential movement compared to stations on either side of the allochthonous units in the Gulf of Cadiz is small to none. No significant motion occurs relative to stations situated to the south (RABT, IFRN), and a differential westward movement of ~ 1 mm/yr between SFER and LAGO, across the northern limit of the allochthonous units, can be attributed to strain accumulation across the seismic belt at the SW-Iberian margin. Instead of subduction, we may expect accommodation of transpression between the Gibraltar arc and Iberia along the SW-Iberian margin and the Azores Gibraltar fracture zone (Sartori et al., 1994), where relevant instrumental seismicity and predominately reverse to strike-slip faulting is observed (Buforn et al., 2004; Stich et al., 2005b).

The first order, long wavelength pattern of the regional GPS velocity field relative to stable Eurasia is simple, and consistent with seismicity (Fig. 8): 1) Intraplate Iberia shows minor, uniform motion, corresponding to overall low seismicity; 2) The anticlockwise rigid

Nubian plate rotation is accommodated to a large extend in Northern Algeria where at least ~ 3 mm/yr of shortening occurs, and partly in the Moroccan Atlas with ~ 2 mm/yr of shortening; 3) In the Alboran–Betic–Gibraltar region, the velocity field shows a clockwise rotation and increasing absolute values, from the barely significant southward motion in the north to the relevant westward residual velocities of the Gibraltar arc. This region appears to be bounded to the east by the TASZ, where seismicity and neotectonics evidence relevant localized shear deformation, contrasting with the compressive Algerian margin further east. The clockwise rotational component of the Alboran–Betic–Gibraltar GPS velocity field is consistent with the observed variety of faulting patterns: In the rear (i.e. north-east), relative motion away from eastern Iberia causes distributed internal deformation and widespread extension in the Betic Range and Alboran basin, and an extensional component of deformation in the TASZ. To the front (i.e. north-west), oblique relative motion towards the SW Iberian margin and northern Atlantic causes a belt of transpressional deformation. Approaching the apparent center line of rotation, velocities and gradients of relative motion become smaller in Western Andalusia, coincident with the lower level of instrumentally recorded seismicity along this sector.

Differential motion and internal deformation of the Alboran–Betic–Gibraltar domain may be seen as a consequence of regional-scale subcrustal dynamic processes, involving several possible scenarios for recycling of lithospheric material in the upper mantle (e.g. Platt and Vissers, 1989; Zeck, 1996; Seber et al., 1996; Lonergan and White, 1997; Morales et al., 1999; Faccenna et al., 2004), or WSW-ward escape processes of fault bounded crustal blocks between the two main plates, at several scales (e.g. Muñoz et al., 2002, Martínez-Díaz and Hernández-Enrile, 2004). In this study, we observed that no significant strain is accumulated along the southern limit of the region between the Gibraltar arc and western Morocco, where the GPS velocity vectors show only a minor ~ 15° rotation compared to theoretical Nubian plate motion. This concurrence leads us to hypothesize a role of the rigid Nubian plate rotation in explaining differential motion of the Alboran–Betic–Gibraltar region: Nubian plate motion, and the associated westward flow pattern in the mantle, may exert a traction on the southern edge of the region (Fig. 8). Such a process might be promoted by mechanical coupling between the crustal and upper mantle strain fields in the presence of old, Jurassic oceanic lithosphere along the passive Atlantic margin, as such a coupling has been inferred from focal mechanism studies along the Iberian section of the margin (Stich et al., 2005b). We want to stress that hypothesizing a possible passive drag of Alboran–Betic–Gibraltar lithosphere by Nubian plate rotation does not contradict other physical mechanisms that have been proposed to explain regional geodynamics, and that may coexist in the region. However, we feel it introduces additional uncertainty about the relative contributions of a number of potential driving mechanisms, and about their possible interaction.

Acknowledgements

High quality seismic broadband data for this study were collected and provided by IAG-Granada, MedNet/INGV, IRIS, Orfeus, Geofon/ROA/UCM, ICC-Barcelona, Observatori de l'Ebre, IST-Lisbon, French RéNaSS, and the temporal TEDESE experiment. We are thankful to all individuals and institutions contributing to GPS data collection and dissemination. Thanks are due to EUREF, ASI-CGS in Matera, UNAVCO and SOPAC for providing permanent GPS data and solutions, and to Giuseppe Casula, Marco Anzidei and Paolo Baldi for support in the GPS data analysis. We acknowledge work on free software GMT (Wessel and Smith, 1998). The study was supported by Spanish project CGL2005-04541-C03-01/BTE, projects RNM104 and RNM00327 of Junta de Andalucía, Consolider "Topo-Iberia" CSD2006-00041, the Italian Civil Protection Department (ES) and European Commission's project SPICE, MRTN-CT-2003-504267 (DS). We particularly appreciate the very detailed and elaborate comments by José Martínez Díaz and an anonymous reviewer, which helped to focus and enrich the manuscript.

References

Aki, K., Richards, P.G., 2002. Quantitative Seismology, 2nd edition. University Science Books, New York.

Altamini, Z., Sillard, P., Boucher, C., 2002. ITRF2000: A new release of the International Terrestrial Reference Frame for earth science applications. J. Geophys. Res. 107 (B10), 2214, doi:10.1029/2001JB000561.

Andeweg, B., Cloetingh, S., 2001. Evidence for an active sinistral shear zone in the western Alboran region. Terra Nova 13, 44–50.

Andeweg, B., de Vicente, G., Cloetingh, S., Giner, J., Muñoz Martin, A., 1999. Local stress field and intraplate deformation of Iberia: variations in spatial and temporal interplay of regional stress sources. Tectonophysics 305, 153–164.

Arboleya, M.L., Teixell, A., Charroud, M., Julivert, M., 2004. A structural transect through the high and middle atlas of Morocco. J. Afr. Earth Sci. 39 (2004), 319–327.

Armijo, R., Flerit, F., King, G.C.P., Meyer, B., 2003. Linear elastic fracture mechanics explains the past and present evolution of the Aegean. Earth Planet. Sci. Lett. 217, 85–95.

Battaglia, M., Murray, M.H., Serpelloni, E., Burgmann, R., 2004. The Adriatic region: an independent microplate within the Africa–

Eurasia collision zone. Geophys. Res. Lett. 31, L09605, doi:10.1029/2004GL019723.
Bell, J.W., Amelung, F., King, G.C.P., 1997. Preliminary late Quaternary slip history of the Carboneras fault, southeastern Spain. J. Geodyn. 24, 51–66.
Bezzeghoud, M., Buforn, E., 1999. Source parameters of the 1992 Melilla (Spain, M_w=4.8), 1994 Alhoceima (Morocco, M_w=5.8), and 1994 Mascara (Algeria, M_w=5.7) earthquakes and seismotectonic implications. Bull. Seismol. Soc. Am. 89, 359–372.
Borges, J.F., Fitas, A.J.S., Bezzeghoud, M., Teves-Costa, P., 2001. Seismotectonics of Portugal and its adjacent Atlantic area. Tectonophysics 337, 373–387.
Bousquet, J.C., 1979. Quaternary strike-slip faults in southeastern Spain. Tectonophysics 52, 277–286.
Braunmiller, J., Bernardi, F., 2005. The 2003 Boumerdes, Algeria earthquake: regional moment tensor analysis. Geophys. Res. Lett. 32, L06305, doi:10.1029/2004GL022038.
Braunmiller, J., Kradolfer, U., Baer, M., Giardini, D., 2002. Regional moment tensor determination in the European–Mediterranean area-initial results. Tectonophysics 356, 5–22.
Buforn, E., Coca, P., 2002. Seismic moment tensor for intermediate depth earthquakes at regional distances in Southern Spain. Tectonophysics 356, 49–63.
Buforn, E., Bezzeghoud, M., Udías, A., Pro, C., 2004. Seismic sources on the Iberia–African plate boundary and their tectonic implications. Pure Appl. Geophys. 161, 623–646.
Buforn, E., Coca, P., Udias, A., Lasa, C., 1997. Source mechanism of intermediate and deep earthquakes in southern Spain. J. Seismol. 1, 113–130.
Buforn, E., Sanz de Galdenao, C., Udías, A., 1995. Seismotectonics of the Ibero–Maghrebian region. Tectonophysics 248, 247–261.
Calais, E., DeMets, C., Nocquet, J.M., 2003. Evidence for a post-3.16-Ma change in Nubia–Eurasia–North America plate motions? Earth Planet. Sci. Lett. 216, 8–92.
Calvert, A., Gomez, F., Seber, D., Barazangi, M., Jabour, N., Ibenbrahim, A., Demnati, A., 1997. An integrated geophysical investigation of recent seismicity in the Al-Hoceima Region of North Morocco. Bull. Seismol. Soc. Am. 87, 637–651.
Calvert, A., Sandvol, E., Seber, D., Barazangi, M., Roecker, S., Mourabit, T., Vidal, F., Alguacil, G., Jabour, N., 2000. Geodynamic evolution of the lithosphere and upper mantle beneath the Alboran region of the western Mediterranean: constraints from travel time tomography. J. Geophys. Res. 105, 10871–10898.
Caporali, A., 2003. Average strain rate in the Italian crust inferred from a permanent GPS network — I. Statistical analysis of the time-series of permanent stations. Geophys. J. Int. 155, 241–253.
Cloetingh, S., Burov, E., Andeweg, B., Beekmann, F., Andriessen, P.A.M., Garcia-Castellanos, D., de Vicente, G., Vegas, R., 2002. Lithospheric folding in Iberia. Tectonics 21, 1041, doi:10.1029/2001TC901031.
Comas, M.C., Platt, J.P., Soto, J.I., Watts, A.B., 1999. The origin and tectonic history of the Alboran Basin: insights from Leg 161 results. In: Zahn, R., Comas, M.C., Klaus, A. (Eds.), Proc. ODP, Sci. Res., vol. 161. Ocean Drilling Program, College Station, TX, pp. 555–580.
D'Agostino, N., Selvaggi, G., 2004. Crustal motion along the Eurasia–Nubia plate-boundary in the Calabrian Arc and Sicily and active extension in the Messina Straits from GPS measurements. J. Geophys. Res. 109, B11402, doi:10.1029/2004JB002998.
De Larouzière, F., de Bolze, J., Bordet, P., Hernandez, J., Montenat, C., Ott d'Estevou, P., 1988. The Betic segment of the lithospheric Trans Alboran shear zone during the Late Miocene. Tectonophysics 152, 41–52.
Delouis, B., Vallée, M., Meghraoui, M., Calais, E., Maouche, S., Lammali, K., Mahsas, A., Briole, P., Benhamouda, F., Yelles, K., 2004. Slip distribution of the 2003 Boumerdes–Zemmouri earthquake, Algeria, from teleseismic, GPS, and coastal uplift data. Geophys. Res. Lett. 31, L18607, doi:10.1029/2004GL020687.
DeMets, C., Gordon, R.G., Argus, D.F., Stein, S., 1994. Effect of recent revisions to the geomagnetic reversal time scale on estimates of current plate motions. Geophys. Res. Lett. 21, 2191–2194.
Dixon, T.H., Miller, M., Farina, F., Wang, H., Johnson, D., 2000. Present-day motion of the Sierra Nevada block and some tectonic implications for the Basin and Range province, North American Cordillera. Tectonics 19 (1), 1–24.
Docherty, C., Banda, E., 1995. Evidence for the eastward migration of the Alboran Sea based on regional subsidence analysis: a case for basin formation by delamination of the subcrustal lithosphere? Tectonics 14, 804–818.
Dong, D., Fang, P., Bock, Y., Cheng, M.K., Miyazaki, S., 2002. Anatomy of apparent seasonal variation from GPS-derived site position. J. Geophys. Res. 107, doi:10.1029/2001JB000573.
Dong, D., Herring, T.A., King, R.W., 1998. Estimating regional deformation from a combination of space and terrestrial geodetic data. J. Geodyn. 72, 200–214.
Dufumier, H., Souriau, A., Sylvander, M., Judenherc, S., Granet, M., 2000. Calculs de magnitudes et mécanismes au foyer pour le séisme de Saint-Béat du 4 Octobre 1999. C. R. Acad. Sci., Paris, 331, 331–338.
Duggen, S., Hoernle, K., van der Bogaard, H., 2004. Magmatic evolution of the Alboran region: the role of subduction in forming the western Mediterranean and causing the Messinian Salinity Crisis. Earth Planet. Sci. Lett. 218, 91–108.
Dziewonski, A.M., Woodhouse, J.H., 1983. An experiment in the systematic study of global seismicity: centroid moment-tensor solutions for 201 moderate and large earthquakes of 1981. J. Geophys. Res. 88, 3247–3271.
Faccenna, C., Piromallo, C., Crespo-Blanc, A., Jolivet, L., Rossetti, F., 2004. Lateral slab deformation and the origin of the western Mediterranean arcs. Tectonics 23, TC1012, doi:10.1029/2002TC001488.
Frizon de Lamotte, D., Andrieux, J., Guézou, J.C., 1991. Cinématique des chevauchements Néogènes dans l'arc bético-Rifains, discussion sue les modèles géodynamiques. Bull. Soc. Geol. Fr. 4, 611–626.
Galindo-Zaldívar, J., Jabaloy, A., Serrano, I., Morales, J., González-Lodeiro, F., Torcal, F., 1999. Recent and present-day stresses in the Granada Basin (Betic Cordilleras): example of a late Miocene-present-day extensional basin in a convergent plate boundary. Tectonics 18, 686–702.
Gephart, J.W., 1990. FMSI: A Fortran program for inverting fault/slickenside and earthquake focal mechanism data to obtain the regional stress tensor. Comput. Geosci. 16, 953–989.
Gomez, F., Beauchamp, W., Barazangi, M., 2000. Role of the Atlas Mountains (northwest Africa) within the African–Eurasian plate-boundary zone. Geology 28, 775–778.
Gràcia, E., Pallàs, R., Soto, J.I., Comas, M., Moreno, X., Masana, E., Santanach, P., Diez, S., García, M., Dañobeitia, J., HITS scientific party, 2005. Active faulting offshore SE Spain (Alboran Sea): implications for earthquake hazard assessment in the Southern Iberian Margin. Earth Planet. Sci. Lett. 241, 734–749.
Gutscher, M.A., Malod, J., Rehault, J.P., Contrucci, I., Klingelhoefer, F., Mendes-Victor, L., Spakman, W., 2002. Evidence for active subduction beneath Gibraltar. Geology 30, 1071–1074.
Hanks, T.C., Kanamori, H., 1979. A moment magnitude scale. J. Geophys. Res. 84, 2348–2350.

Herraiz, M., De Vicente, G., Lindo-Naupari, R., Giner, J., Simón, J.L., González-Casado, J.M., Vadillo, O., Rodríguez-Pascua, M.A., Cicuéndez, J.I., Casas, A., Cabañas, L., Rincón, P., Cortés, A.L., Ramírez, M., Lucini, M., 2000. The recent (upper Miocene to Quaternary) and present tectonic stress distributions in the Iberia Peninsula. Tectonics 19, 762–786.

Herring, T.A., 2004. GLOBK: Global Kalman Filter VLBI and GPS Analysis Program Version 10.0. Massachusetts Institute of Technology, Cambridge.

Hoernle, K., Zhang, Y.S., Graham, D., 1995. Seismic and geochemical evidence for large-scale mantle upwelling beneath the eastern Atlantic and western and central Europe. Nature 374, 34–39.

Jolivet, L., Faccenna, C., 2000. Mediterranean extension and the Africa–Eurasia collision. Tectonics 19, 1095–1106.

Julià, J., Mancilla, F., Morales, J., 2005. Seismic signature of intracrustal magmatic intrusions in the Eastern Betics (Internal Zone), SE Iberia. Geophys. Res. Lett. 32, L16304, doi:10.1029/2005GL023274.

King, R.W., Bock, Y., 2004. Documentation for GAMIT GPS Analysis Software, Version 10.01. Massachusetts Institute of Technology and Scripps Institution of Oceanography.

Kreemer, C., Holt, W.E., Haines, A.J., 2003. An integrated global model of present-day plate motions and plate-boundary deformation. Geophys. J. Int. 154, 8–34.

Langston, C.A., Barker, J.S., Pavlin, G.B., 1982. Point-source inversion techniques. Phys. Earth Planet. Int. 30, 228–241.

Leblanc, D., Olivier, P., 1984. Role of strike-slip faults in the Betic–Rifian Orogeny. Tectonophysics 101, 345–355.

Lonergan, L., White, N., 1997. Origin of the Betic–Rif mountain belt. Tectonics 16, 504–522.

Mancilla, F., Ammon, C.J., Herrmann, R.B., Morales, J., 2002. Faulting parameters of the 1999 Mula earthquake, southeastern Spain. Tectonophysics 354, 139–155.

Mantovani, E., Viti, M., Cenni, N., Albarello, D., Babbucci, D., 2001. Short and long term deformation patterns in the Aegean–Anatolian systems: insights from space geodetic data (GPS). Geophys. Res. Lett. 28, 2325–2328.

Mao, A., Harrison, C.G.A., Dixon, T.H., 1999. Noise in GPS coordinate time series. J. Geophys. Res. 104, 2797–2816.

Martínez-Díaz, J.J., 2002. Stress field variations related to fault interaction in a reverse oblique-slip fault: the Alhama de Murcia fault, Betic Cordillera, Spain. Tectonophysics 356, 291–305.

Martínez-Díaz, J.J., Hernández-Enrile, J.L., 2004. Neotectonics and morphotectonics of the southern Almería region (Betic Cordillera–Spain) kinematics implications. Int. J. Earth Sci. 93, 189–206.

Masana, E., Martínez-Díaz, J.J., Hernández-Enrile, J.L., Santanach, P., 2004. The Alhama de Murcia fault (SE Spain), a seismogenic fault in a diffuse plate boundary: seismotectonic implications for the Ibero–Magrebian region. J. Geophys. Res. 109, B01301, doi:10.1029/2002JB002359.

Masana, E., Pallàs, R., Perea, H., Ortuño, M., Martínez-Díaz, J.J., García-Meléndez, E., Santanach, P., 2005. Large Holocene morphogenic earthquakes along the Albox fault, Betic Cordillera, Spain. J. Geodyn. 40, 119–133.

McClusky, S., et al., 2000. Global Positioning System constraints on plate kinematics and dynamics in the eastern Mediterranean and Caucasus. J. Geophys. Res. 105, 5695–5719.

McClusky, S., Reilinger, R., Mahmoud, S., Ben Sari, D., Tealeb, A., 2003. GPS constraints on Africa (Nubia) and Arabia plate motions. Geophys. J. Int. 155, 126–138.

McKenzie, D.P., 1969. The relationship between fault plane solutions for earthquakes and the directions of the principal stresses. Bull. Seismol. Soc. Am. 59, 591–601.

Meade, B.J., Hager, B.H., Reilinger, R.E., 2002. Estimates of seismic potential in the Marmara region from block models of secular deformation constrained by GPS measurements. Bull. Seismol. Soc. Am. 92, 208–215.

Mezcua, J., Rueda, J., 1997. Seismological evidence for a delamination process in the lithosphere under the Alboran Sea. Geophys. J. Int. 129, 1–8.

Montenat, C., Ott D'Estevou, P., La Chappelle, G., 1990. Le Bassin de Nijar-Carboneras et le Couloir du Bas-Andarax, Documents et Travaux. Int. Geol. Albert Lapparent 12–13, 129–164.

Morales, J., Vidal, F., de Miguel, F., Alguacil, G., Posadas, A.M., Ibáñez, J.M., Guzmán, A., Guirao, J.M., 1990. Basement structure of the Granada basin, Betic Cordilleras, Southern Spain. Tectonophysics 177, 337–348.

Morales, J., Serrano, I., Vidal, F., Torcal, F., 1997. The depth of the earthquake activity in the Central Betics (southern Spain). Geophys. Res. Lett. 24, 3289–3292.

Morales, J., Serrano, I., Jabaloy, A., Galindo-Zaldivar, J., Zhao, D., Torcal, F., Vidal, F., Gonzalez-Lodeiro, F., 1999. Active continental subduction beneath the Betic Cordillera and Alboran Sea. Geology 27, 735–738.

Muñoz, D., Cisternas, A., Udías, A., Mezcua, J., Sanz de Galdeano, C., Morales, J., Sánchez-Venero, M., Haessler, H., Ibañez, J., Buforn, E., Pascual, G., Rivera, L., 2002. Microseismicity and tectonics in the Granada Basin (Spain). Tectonophysics 356, 233–252.

Nocquet, J.M., Calais, E., 2003. Crustal velocity field of western Europe from permanent GPS array solutions, 1996–2001. Geophys. J. Int. 154, 72–88.

Nyst, M., Thatcher, W., 2003. New constraints on the active tectonic deformation of the Aegean. J. Geophys. Res. 109 (B11), B11406, doi:10.1029/2003JB002830.

Platt, J.P., Vissers, R.L.M., 1989. Extensional collapse of thickened continental lithosphere: A working hypothesis for the Alboran sea and Gibraltar arc. Geology 17, 540–543.

Platt, J.P., Allerton, S., Kirker, A., Mandeville, C., Mayfield, A., Platzman, E.S., Rimi, A., 2003. The ultimate arc: differential displacement, oroclinal bending, and vertical axis rotation in the external Betic–Rif arc. Tectonics 22, 1017, doi:10.1029/2001TC001321.

Pondrelli, S., Ekström, G., Morelli, A., Primerano, S., 1999. Study of source geometry for tsunamigenic events of the Euro-Mediterranean area. International Conference on Tsunamis. UNESCO Books, Paris, pp. 297–307.

Pondrelli, S., Morelli, A., Ekström, G., Mazza, S., Boschi, E., Dziewonski, A.M., 2002. European–Mediterranean regional centroid-moment tensors: 1997–2000. Phys. Earth Planet. Int. 130, 71–101.

Randall, G.E., 1994. Efficient calculation of complete differential seismograms for laterally homogeneous earth models. Geophys. J. Int. 118, 245–254.

Randall, G.E., Ammon, C.J., Owens, T.J., 1995. Moment tensor estimation using regional seismograms from a Tibetan Plateau portable network deployment. Geophys. Res. Lett. 22, 1665–1668.

Rigo, A., Souriau, A., Dubos, N., Sylvander, M., Ponsolles, C., 2005. Analysis of the seismicity in the central part of the Pyrenees (France), and tectonic implications. J. Seismol. 9, 211–222.

Rueda, J., Mézcua, J., 2005. Near-real-time seismic moment-tensor determination in Spain. Seismol. Res. Lett. 76, 455–465.

Sanz de Galdeano, C., 1990. Geologic evolution of the Betic Cordilleras in the Western Mediterranean, Miocene to the present. Tectonophysics 172, 107–119.

Sartori, R., Torelli, L., Zitellini, N., Peis, D., Lodolo, E., 1994. Eastern segment of the Azores–Gibraltar line (central-eastern Atlantic): an

oceanic plate boundary with diffuse compressional deformation. Geology 22, 555–558.

Seber, D., Barazangi, M., Ibenbrahim, A., Demnati, A., 1996. Geophysical evidence for lithospheric delamination beneath the Alboran Sea and Rif–Betic mountains. Nature 379, 785–790.

Sella, G.F., Dixon, T.H., Mao, A., 2002. REVEL: a model for recent plate velocities from space geodesy. J. Geophys. Res. 107 (B4), doi:10.1029/2000JB000033.

Serpelloni, E., Anzidei, M., Baldi, P., Casula, G., Galvani, A., Pesci, A., Riguzzi, F., 2002. Combination of permanent and non-permanent GPS networks for the evaluation of the strain-rate field in the central Mediterranean area. Boll. Geofis. Teor. Appl. 43, 195–219.

Serpelloni, E., Anzidei, M., Baldi, P., Casula, G., Galvani, A., 2005. Crustal velocity and strain-rate fields in Italy and surrounding regions: new results from the analysis of permanent and non-permanent GPS networks. Geophy. J. Int. 161 (3), 861–880.

Serpelloni, E., Casula, G., Galvani A., Anzidei M., Baldi P., in press. Data analysis of permanent GPS networks in Italy and surrounding regions: application of a distributed processing approach. Ann. Geophys.

Serpelloni, E., Vannucci, G., Pondrelli, S., Argnani, A., Casula, G., Anzidei, M., Baldi P., Gasperini P., submitted for publication. The Northern Africa Plate-Boundary in the Western and Central Mediterranean: new Constraints From Earthquake Focal Mechanisms and GPS Data. Geophys. J. Int.

Serrano, I., Morales, J., Zhao, D., Torcal, F., Vidal, F., 1998. P-wave tomographic images of the central Betics–Alboran Sea (southern Spain) using local earthquakes: contribution for a continental collision. Geophys. Res. Lett. 25, 4031–4034.

Shen, Z.-K., Jackson, D.D., Ge, X.B., 1996. Crustal deformation across and beyond the Los Angeles basin from geodetic measurements. J. Geophys. Res. 101, 27, 957–27, 980.

Silva, P.G., Goy, J.L., Somoza, L., Zazo, C., Bardají, T., 1993. Landscape response to strike-slip faulting linked to collisional settings: quaternary tectonics and basin formation in the Eastern Betics, southeastern Spain. Tectonophysics 224, 289–303.

Silver, P.G., Jordan, T.H., 1982. Optimal estimation of scalar seismic moment. Geophys. J. R. Astron. Soc. 70, 755–787.

Stich, D., Ammon, C.J., Morales, J., 2003. Moment tensor solutions for small and moderate earthquakes in the Ibero–Maghreb region. J. Geophys. Res. 108, 2148, doi:10.1029/2002JB002057.

Stich, D., Mancilla, F., Baumont, D., Morales, J., 2005a. Source analysis of the M_w 6.3 2004 Al Hoceima earthquake (Morocco) using regional apparent source time functions. J. Geophys. Res. 110, B06306, doi:10.1029/2004JB003366.

Stich, D., Mancilla, F., Morales, J., 2005b. Crust–mantle coupling in the Gulf of Cadiz (SW-Iberia). Geophys. Res. Lett. 32, L13306, doi:10.1029/2005GL023098.

Stich, D., Batlló, J., Macià, R., Teves-Costa, P., Morales, J., 2005c. Moment tensor inversion with single-component historical seismograms: the 1909 Benavente (Portugal) and Lambesc (France) earthquakes. Geophys. J. Int. 162, 850–858.

Thiebot, E., Gutscher M.A., in press. The Gibraltar Arc seismogenic zone (part 1): constraints on a shallow east dipping fault plane source for the 1755 Lisbon earthquake provided by seismic data, gravity and thermal modelling. Tectonophysics. (Corrected Proof, Available online 10 July 2006).

Thio, H.K., Song, X., Saikia, C.K., Helmberger, D.V., Woods, B.B., 1999. Seismic source and structure estimation in the western Mediterranean using a sparse broadband network. J. Geophys. Res. 104, 845–861.

Torné, M., Fernàndez, M., Comas, M.C., Soto, J.I., 2000. Lithospheric structure beneath the Alboran Basin: results from 3D gravity modeling and tectonic relevance. J. Geophys. Res. 105, 3209–3228.

Vannucci, G., Gasperini, P., 2004. The new release of the database of Earthquake Mechanisms of the Mediterranean Area (EMMA Version 2). Ann. Geophys. 47, 307–334 (Suppl. S).

Vegas, R., Banda, E., 1982. Tectonic framework and Alpine evolution of the Iberian Peninsula. Earth Evol. Sci. 4, 320–343.

Wessel, P., Smith, W.H.F., 1998. New, improved version of the Generic Mapping Tools released. EOS Trans. AGU 79, 579.

Zeck, H.P., 1996. Betic–Rif orogeny: subduction of Mesozoic Tethys lithosphere under eastward drifting Iberia, slab detachment shortly before 22 Ma, and subsequent uplift and extensional tectonics. Tectonophysics 254, 1–16.

Zitellini, N., Rovere, M., Terrinha, P., Chierici, F., Matias, L., BIGSETS Team, 2004. Neogene through quaternary tectonic reactivation of SW Iberian passive margin. Pure Appl. Geophys. 161, 565–587.